

RESEARCH ARTICLE

In silico analysis of the V66M variant of human BDNF in psychiatric disorders: An approach to precision medicine

Clara Carolina Silva De Oliveira¹✉, Gabriel Rodrigues Coutinho Pereira¹✉, Jamile Yvis Santos De Alcantara¹†, Deborah Antunes¹‡, Ernesto Raul Caffarena²‡, Joelma Freire De Mesquita¹✉*

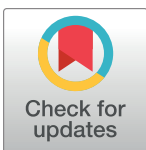
1 Department of Genetics and Molecular Biology, Bioinformatics and Computational Biology Laboratory, Federal University of the State of Rio de Janeiro (UNIRIO), Rio de Janeiro, Rio de Janeiro, Brazil,

2 Computational Biophysics and Molecular Modeling Group, Scientific Computing Program (PROCC), Fundação Oswaldo Cruz, Manguinhos, Rio de Janeiro, Brazil

✉ These authors contributed equally to this work.

† These authors also contributed equally to this work.

* joelma.mesquita@unirio.br



OPEN ACCESS

Citation: De Oliveira CCS, Pereira GRC, De Alcantara JYS, Antunes D, Caffarena ER, De Mesquita JF (2019) *In silico* analysis of the V66M variant of human BDNF in psychiatric disorders: An approach to precision medicine. PLoS ONE 14(4): e0215508. <https://doi.org/10.1371/journal.pone.0215508>

Editor: Alexandre G. de Brevern, UMR-S1134, INSERM, Université Paris Diderot, INTS, FRANCE

Received: January 17, 2018

Accepted: April 4, 2019

Published: April 18, 2019

Copyright: © 2019 De Oliveira et al. This is an open access article distributed under the terms of the [Creative Commons Attribution License](#), which permits unrestricted use, distribution, and reproduction in any medium, provided the original author and source are credited.

Data Availability Statement: All relevant data are within the paper.

Funding: This work was supported by FAPERJ - Fundação Carlos Chagas Filho de Amparo à Pesquisa do Estado do Rio de Janeiro (<http://www.faperj.br/>) FINEP - Financiadora de Estudos e Projetos (<http://www.finep.gov.br/>) CAPES - Coordenação de Aperfeiçoamento de Pessoal de Nível Superior (<http://www.capes.gov.br/>), and CNPq - Conselho Nacional de Desenvolvimento

Abstract

Brain-derived neurotrophic factor (BDNF) plays an important role in neurogenesis and synapse formation. The V66M is the most prevalent BDNF mutation in humans and impairs the function and distribution of BDNF. This mutation is related to several psychiatric disorders. The pro-region of BDNF, particularly position 66 and its adjacent residues, are determinant for the intracellular sorting and activity-dependent secretion of BDNF. However, it has not yet been fully elucidated. The present study aims to analyze the effects of the V66M mutation on BDNF structure and function. Here, we applied nine algorithms, including SIFT and PolyPhen-2, for functional and stability prediction of the V66M mutation. The complete theoretical model of BDNF was generated by Rosetta and validated by PROCHECK, RAM-PAGE, ProSa, QMEAN and Verify-3D algorithms. Structural alignment was performed using TM-align. Phylogenetic analysis was performed using the ConSurf server. Molecular dynamics (MD) simulations were performed and analyzed using the GROMACS 2018.2 package. The V66M mutation was predicted as deleterious by PolyPhen-2 and SIFT in addition to being predicted as destabilizing by I-Mutant. According to SNPeffect, the V66M mutation does not affect protein aggregation, amyloid propensity, and chaperone binding. The complete theoretical structure of BDNF proved to be a reliable model. Phylogenetic analysis indicated that the V66M mutation of BDNF occurs at a non-conserved position of the protein. MD analyses indicated that the V66M mutation does not affect the BDNF flexibility and surface-to-volume ratio, but affects the BDNF essential motions, hydrogen-bonding and secondary structure particularly at its pre and pro-domain, which are crucial for its activity and distribution. Thus, considering that these parameters are determinant for protein interactions and, consequently, protein function; the alterations observed throughout the MD analyses may be related to the functional impairment of BDNF upon V66M mutation, as well as its involvement in psychiatric disorders.

Científico e Tecnológico (<http://cnpq.br/>) to CCSDO. We gratefully acknowledge the support of NVIDIA Corporation with their donation of the Titan X Pascal GPU used for this research. The funders had no role in study design, data collection and analysis, decision to publish, or preparation of the manuscript.

Competing interests: NVIDIA's GPU Grant Program recently donated (1) Titan X Pascal GPU for our research group. This donation is an unrestricted gift to support our research efforts and comes at no charge. There are no patents, products in development or marketed products to declare. This does not alter our adherence to all the PLOS ONE policies on sharing data and materials.

Introduction

Psychiatric disorders are polygenic and multifactorial brain syndromes [1] characterized by clinically significant behavioral, psychological or biological dysfunction [2]. Psychiatric disorders are considered a major public health problem and are responsible for severe distress and functional impairment in individuals with notorious consequences in those who have been affected and their families and social and work environments [3]. Although the global burden of psychiatric disorders is mainly assigned to the disability and not to the mortality of affected individuals [4], mortality rates in psychiatric patients are much higher than those reported in the general population [5,6]. It is estimated that more than 50% of the population in middle and high-income countries will suffer from at least one psychiatric disorder throughout life. In addition, the estimated cost of these diseases between 2011 and 2030 is thereby projected at US \$ 16.3 trillion dollars, which makes the economic cost of psychiatric disorders comparable to that of cardiovascular diseases and higher than that of cancer, diabetes and chronic respiratory diseases [3].

Although there is no consensus on the cause of psychiatric disorders [1,7], most studies suggest they are caused by neurotransmitters deregulation, genetic abnormalities, and defects in the structure or function of the brain [7]. In this context, non-synonymous mutations in the *BDNF* gene are implicated in the development of psychiatric disorders because they affect the function and distribution of brain-derived neurotrophic factor (BDNF), which is crucial for central nervous system development, neurogenesis and neuronal plasticity [8].

BDNF is a 247-amino acid secretory protein encoded by the *BDNF* gene [9], which is located on chromosome 11p14.1 [10]. BDNF is synthesized as a precursor protein, pre-pro-BDNF, which is cleaved into pro-BDNF in the endoplasmic reticulum (ER). Pro-BDNF is addressed and might be further cleaved into mature BDNF (m-BDNF) inside vesicles in the trans-Golgi network. Both dimeric pro-BDNF or dimeric m-BDNF are secreted [8] through activity-dependent exocytosis in excitable cells secreting granules or through constitutive release in all cell types [11]. The secreted homodimers bind to their cognate receptor tropomyosin kinase (Trk) and p75 neurotrophin receptor [12], inducing a series of intracellular signaling cascades related to proliferation, maturation, and maintenance of the neuronal function [8,13].

The most frequent missense mutation of BDNF in humans occurs in the pro-region of the protein [10] and comprises the substitution of a valine to a methionine at position 66 (V66M) [13]. The pro-region of BDNF, particularly the position 66 and its adjacent residues, are determinant for the intracellular sorting and activity-dependent secretion of this molecule [14]. The V66M mutation is believed to impair protein function and distribution [14,15] by interrupting folding, dimerization and intracellular trafficking of the protein [16], in addition to preventing the release-dependent activation of BDNF [14]. This mutation is also associated with the development of bipolar disorder, depression, obsessive-compulsive disorder, eating disorders, schizophrenia [15], anxiety, addiction, and memory and learning disabilities [13]. The structure of the residues 136 to 244 of BDNF have been solved by X-ray crystallography (PDB ID: 1BND and 1B8M) [17]. However, there is no experimentally determined structure for the V66M mutation and its adjacent residues [17].

Knowledge of three-dimensional structures is essential for understanding the mechanisms by which proteins perform their functions [18] and how these mechanisms can be disrupted by disease-associated mutations [19]. However, the determination of protein structures by conventional methods, such as X-ray diffraction and nuclear magnetic resonance (NMR), is expensive and time-consuming [20], increasing the imbalance between the amount of structures elucidated by experimental methods and the number of protein sequences [18] determined by rapid, massively parallel and low-cost sequencing methods [19]. In this scenario,

computational (*in silico*) approaches, are efficient [20] and necessary to predict protein structures [18] and study disease-associated mutations [19] because they enable modeling of three-dimensional structures and prediction of the effect of mutations on protein function based on the amino acid sequence, in a cheaper, faster, and more accurate way when compared to experimental methods [18,20].

In addition to contributing to the development of pathologies [21], missense mutations can also influence the treatment regimen adopted. Understanding the effects of such mutations on the structure and function of a protein is important for precision medicine and the development of new drugs [22]. The characterization of biochemical and structural parameters constitutes the main approach used to understand the functional effects of missense mutations [19]. Despite the central role of BDNF in psychiatric disorders development, little is known about the structural and functional effects of its mutations.

In this work, we used the computational methodology previously described by our group [20,23–25] to analyze the structural and functional effects of the V66M variant of BDNF, which has been associated with several psychiatric disorders [13].

Materials and methods

Dataset

Sequences and information about BDNF and its natural variant V66M were retrieved from the UniProt [9] (UniProt ID: P23560), OMIM (OMIM ID: 113505) [26] and PubMed [10] databases. The BDNF crystallographic structure with the highest resolution on the Protein Data Bank (PDB) database [17] (PDB ID: 1BND) was selected as the modeling template [27].

Functional and stability prediction analysis

The functional and stability effects of the V66M mutation were predicted using the following algorithms: PhD-SNP [28], PMut [29], PolyPhen-2 [30], SIFT [31], SNAP [32], SNPS&GO [33], VarMod [34], SNPeffect4.0 [22] and I-Mutant2.0 [35].

Structural modeling

Complete three-dimensional structures of BDNF were created using *ab initio* and comparative modeling strategies. The algorithms HHpred [36], M4T [37], RaptorX [38] and SwissModel [39] were used for comparative modeling, while Rosetta [40], I-Tasser [41] and Phyre2 [42] algorithms were used for both *ab initio* and comparative modeling. The generated models were structurally aligned to the BDNF crystallographic structure (PDB ID: 1BND) using the TM-align server. The most accurate structure was selected based on the root-mean-square-deviation (RMSD) < 2.0 Å and TM-score values closer to 1 [20].

Structure validation

The selected structure had its quality validated by PROCHECK [43], ProSA [44], Verify-3D [45], RAMPAGE [46], and QMEAN [47] servers. We predicted the secondary structure of BDNF using CONCORD [48]. To further validate the *in silico* modeled structure of BDNF, we compared its secondary structure with the 1BND experimental fragment and with the CONCORD prediction [48].

Phylogenetic analysis

The ConSurf [49] server was used to calculate the evolutionary conservation degree of each amino acid of BDNF. The following parameters were selected for phylogenetic analysis:

homologous search algorithm: CSI-BLAST; number of iterations: 3; E-value cut-off: 0.0001; protein database: UNIREF-90; number of reference sequences selected: 150; maximum sequence identity: 95%; minimum identity for counterparts: 35%; alignment method: Bayesian; calculation method: MAFFT-L-INS-i; and evolutionary substitution model: best model.

Molecular dynamics

Mutator Plugin1.3 [50], available in the Visual Molecular Dynamics (VMD) 4.5 software package [51], was used to induce the V66M substitution on the validated model of BDNF.

Molecular dynamics (MD) simulations of wild-type BDNF and its natural variant V66M were performed in triplicates using the GROMACS 2018.2 package [52]. Amber99SB-ILDN [53] was selected as the force field of the simulations. The structures were solvated using TIP3P water in a dodecahedral box with the dimensions of 55.0 x 82.7 x 45.6 Å. The MD simulation system was neutralized by adding 93 Na⁺ and 96 Cl⁻ ions. The salt concentrations of the system were set to 0.15 mol/l. The system was then minimized in 5000 steps using the steepest descent method.

After system minimization, three other steps were conducted in the MD simulation: NVT (constant number of particles, volume, and temperature), NPT (constant number of particles, pressure, and temperature) and production. The NVT simulation was followed by the NPT simulation at a temperature of 300 K and 1 atmosphere for a duration of 100 ps [20]. In these simulations, all bonds were constrained in the protein to promote position restraint of this group. The position-restrained NVT and NPT prompted water relaxation around the protein and reduced system entropy. Parrinello-Rahman was selected as the barostat of the MD, whereas v-rescale was selected as the thermostat. The barostat and thermostat relaxation lasted 100 ps each.

The production simulation was performed at 300 K for 200 ns for the wild-type BDNF and its V66M variant. The LINCS (linear constraint solver) algorithm was applied to constrain covalent bonds [54]. The electrostatic interactions were processed using the particle mesh Ewald (PME) method [55]. A time step of 0.002 ps was selected for the simulations, and no constant forces were applied. The MD trajectories were recorded every 10 ps [20].

Trajectory analysis

Root-mean-square deviation (RMSD), root-mean-square fluctuation (RMSF), B-factor, radius of gyration (Rg), solvent accessible surface area (SASA), and secondary structure were calculated separately for each triplicate trajectory, taking the initial structure of the production dynamics as the reference, to investigate biochemical and structural changes of the native and mutant structures. The following GROMACS distribution programs were applied to perform these analyses: *gmx rms*, *gmx rmsf*, *gmx gyrate*, *gmx sasa*, and *gmx do_dssp*. The means and their respective confidence interval (0.95) were calculated for each triplicate in the RMSD, Rg and SASA analyses using the *ggplot2* package in R software [56]. PCA analysis was carried out on all systems using the Bio3D library implemented in R [57]. The full three independent MD simulations were concatenated, and trajectory analyses were conducted for native and mutant structures systems. Rotational and translational motions were removed before calculation of the covariance matrix by least-squares superposition to the corresponding average structures. The 3N×3N covariance matrices of Cα atomic positions (Cartesian coordinates) were then calculated for each state.

VMD software was used to calculate distances between atoms and determine hydrogen bond formation using a geometrical criterion. A hit was computed when the distance between two polar heavy atoms, with at least one hydrogen atom attached, was less than 3.5 Å using a D-H-A angle cutoff of 30°.

Results

Functional and stability prediction analysis

PhD-SNP, PMut, PolyPhen-2, SIFT, SNAP, SNPS&GO, and Varmod were used to predict putative deleterious or neutral effects of the V66M mutation on protein function [24]. The variant V66M was predicted as deleterious by SIFT and PolyPhen-2, whereas it was predicted as neutral by PhD-SNP, PMut, SNAP, SNPS&GO, and Varmod.

SNPeffect 4.0 is a four-algorithm method used for phenotyping human mutations [22]. The algorithms WALTZ, TANGO, and LIMBO were used to predict the effects of the V66M mutation on aggregation tendency (TANGO), amyloid propensity (WALTZ) and chaperone binding tendency (LIMBO). The results indicated that the V66M mutation does not alter these characteristics.

FoldX, the fourth SNPeffect 4.0 algorithm, and I-Mutant2.0 algorithms were used to predict the effects of V66M mutation on protein stability. According to FoldX, the V66M mutation does not change protein stability ($\Delta\Delta G = -0.04$ kcal/mol), whereas for I-Mutant, the V66M mutation decreases protein stability ($\Delta\Delta G = -0.49$ kcal/mol).

Structural modeling

The 1BND structure from the Protein DataBank was selected as template for the structural alignment in TM-align because it has the same sequence coverage and better resolution [27] (2.30 Å) than the only other BDNF structural fragment (1B8M, 2.75 Å) [17].

The generated models using HHpred [36], M4T [37], RaptorX [38], SwissModel [39], Rosetta [40], I-Tasser [41] and Phyre2 [42] were structurally aligned to the 1BND crystallographic fragment of BDNF on the TM-align server. The alignment provides two distinct values: RMSD and TM-score, which are parameters used to evaluate structural similarity [58]. Accurate models present TM-scores approaching 1 and RMSD < 2.0 Å [20]. Table 1 shows the RMSD and TM-Score values of the structural alignment.

The algorithms generated accurate models according to the RMSD and TM-scores presented in Table 1. HHpred and SwissModel structures presented the best scores, but these structures were not considered for further analyses because these algorithms generated incomplete models of BDNF.

Amongst the complete generated BDNF structural models, the one provided by Rosetta (Fig 1) presented similar structure to its template and RMSD of 1.04 Å and a TM-score of 0.94492 (Fig 2). Therefore, the Rosetta model was considered the most accurate and selected for structural validation.

Structure validation

The Rosetta structure had its quality validated by PROCHECK [43], ProSA [44], Verify-3D [45], RAMPAGE [46], and QMEAN [47] servers.

Table 1. Structural alignment of the generated models of BDNF and the 1BND fragment.

Modeling Algorithms	RMSD (Å)	TM-Score
HHPred	0.53	0.98489
I-Tasser	1.40	0.89691
M4T	1.21	0.93869
Phyre2	1.65	0.90354
RaptorX	1.21	0.93869
Rosetta	1.04	0.94492
SwissModel	1.05	0.95347

<https://doi.org/10.1371/journal.pone.0215508.t001>

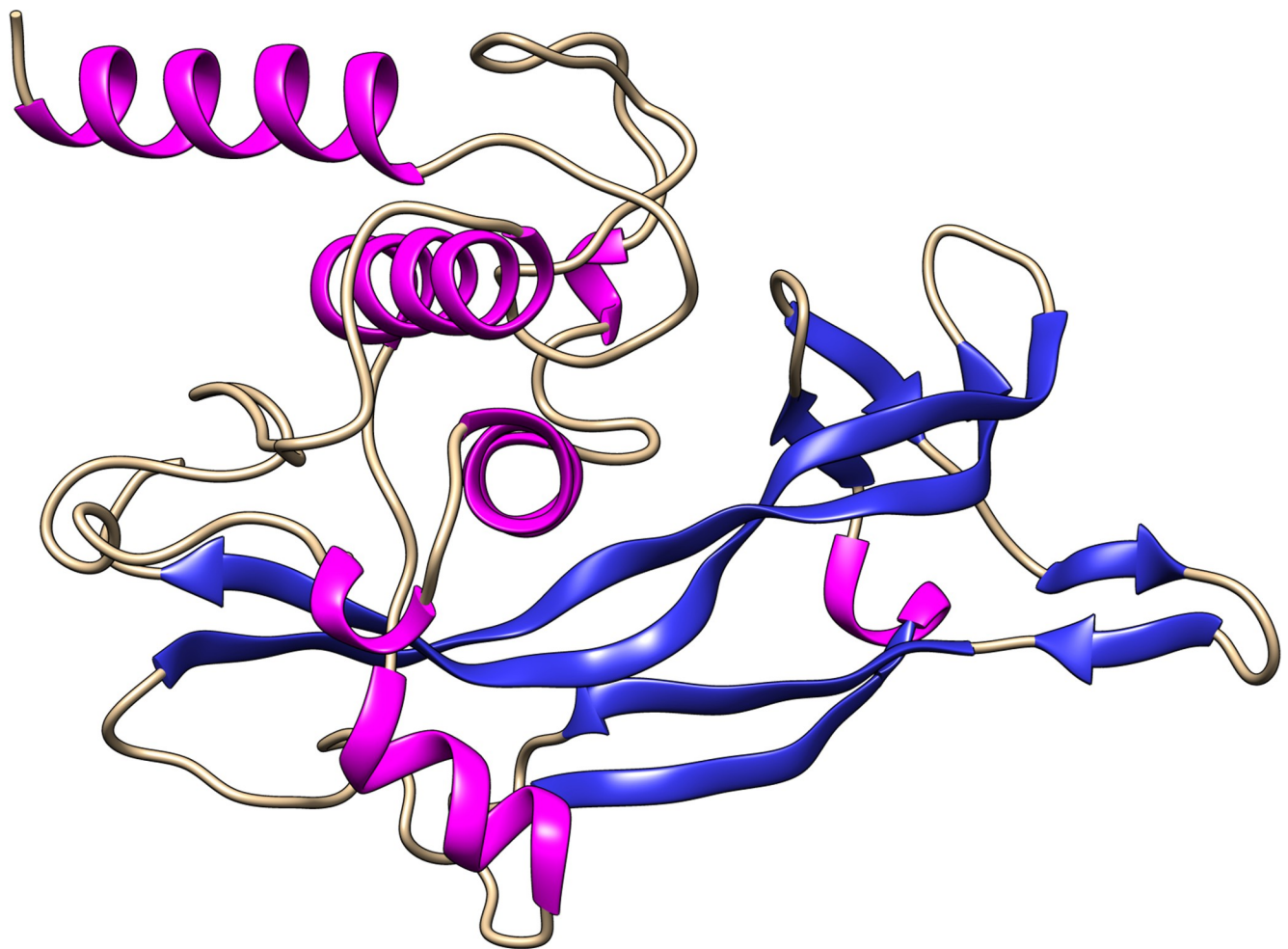


Fig 1. *In silico* modeled structure of BDNF by Rosetta. Secondary structure representation of the *in silico* modeled structure of BDNF generated by Rosetta. The α -helices are represented by pink ribbons, the β -strands are represented by blue arrows, and the coiled regions are represented in beige.

<https://doi.org/10.1371/journal.pone.0215508.g001>

ProSa evaluates the quality of the submitted model by calculating its potential energy and comparing the obtained score with those of the experimental structures deposited in PDB [44]. According to ProSa, the *in silico* structure of BDNF presented a Z-score of -6.24, which is comparable to that of NMR structures of the same size (Fig 3A).

QMEAN estimates the quality of the submitted model based on its physicochemical properties and then generates a value referring to the overall quality of the structure and set it against the calculated QMEAN-scores of 9766 high-resolution experimental structures [47]. According to QMEAN, the *in silico* structure of BDNF presented a QMEAN-score of -1.13, which is comparable to that of high-resolution experimental structures (Fig 3B).

Verify3D assesses the local quality of the submitted model based on its structure-sequence compatibility to generate a compatibility value for each residue of the protein. High-quality structures are expected to present more than 80% of their residues with a 3D-1D score equal to or higher than 0.2 [45]. The *in silico* structure of BDNF presents 3D-1D scores of 0.2 or higher (Fig 2C) in 80.57% of its residues, thus it is considered a high-quality model.

PROCHECK and RAMPAGE evaluate the stereochemical quality of the submitted models based on its phi/psi angle arrangement and then generates Ramachandran plots in which the

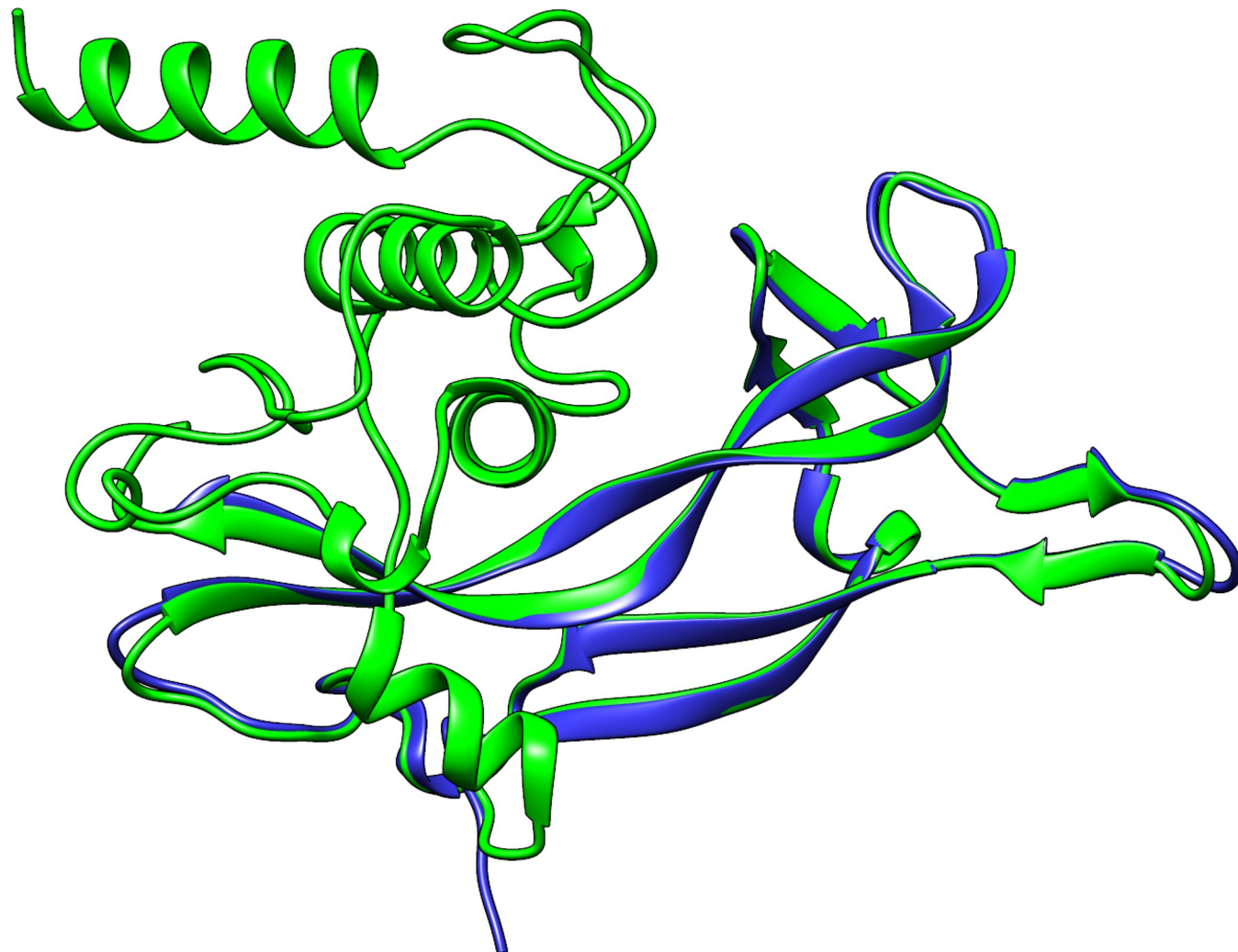


Fig 2. Structural alignment between the theoretical model of BDNF, generated by the Rosetta algorithm, and the experimental fragment of BDNF (PDB ID: 1BND). Cartoon representation of BDNF modeled structure created by Rosetta (green) and the experimental fragment 1BND (blue). The α -helices are represented by ribbons, while the β -strands are represented by arrows.

<https://doi.org/10.1371/journal.pone.0215508.g002>

protein residues are placed on favored, allowed and not allowed regions. For PROCHECK and RAMPAGE, high-quality models are expected to have more than 90% of their residues in the most favored regions of PROCHECK's Ramachandran plot and approximately 98% of their residues in the favored regions of RAMPAGE's Ramachandran plot [43,46]. The predicted model of BDNF shows 90.8% of its residues in the most favored regions of PROCHECK's Ramachandran plot and 97.1 of its residues in the favored region of the RAMPAGE's Ramachandran plot. Thus, it is considered a high-quality model (Fig 4).

Moreover, the secondary structure of human BDNF was predicted by CONCORD, a consensus method that is based on seven secondary structure prediction methods: SSpro, DSC, PROF, PROFphd, PSIPRED, Predator, and GorIV [48]. To further validate the *in silico* modeled structure of BDNF, we compared its secondary structure with the 1BND experimental fragment and with the CONCORD results. This comparison is shown in Fig 5, and indicates that the theoretical model of BDNF also has a high accuracy regarding its secondary structure. The ALINE software [59] was used to generate the secondary structure comparison scheme.

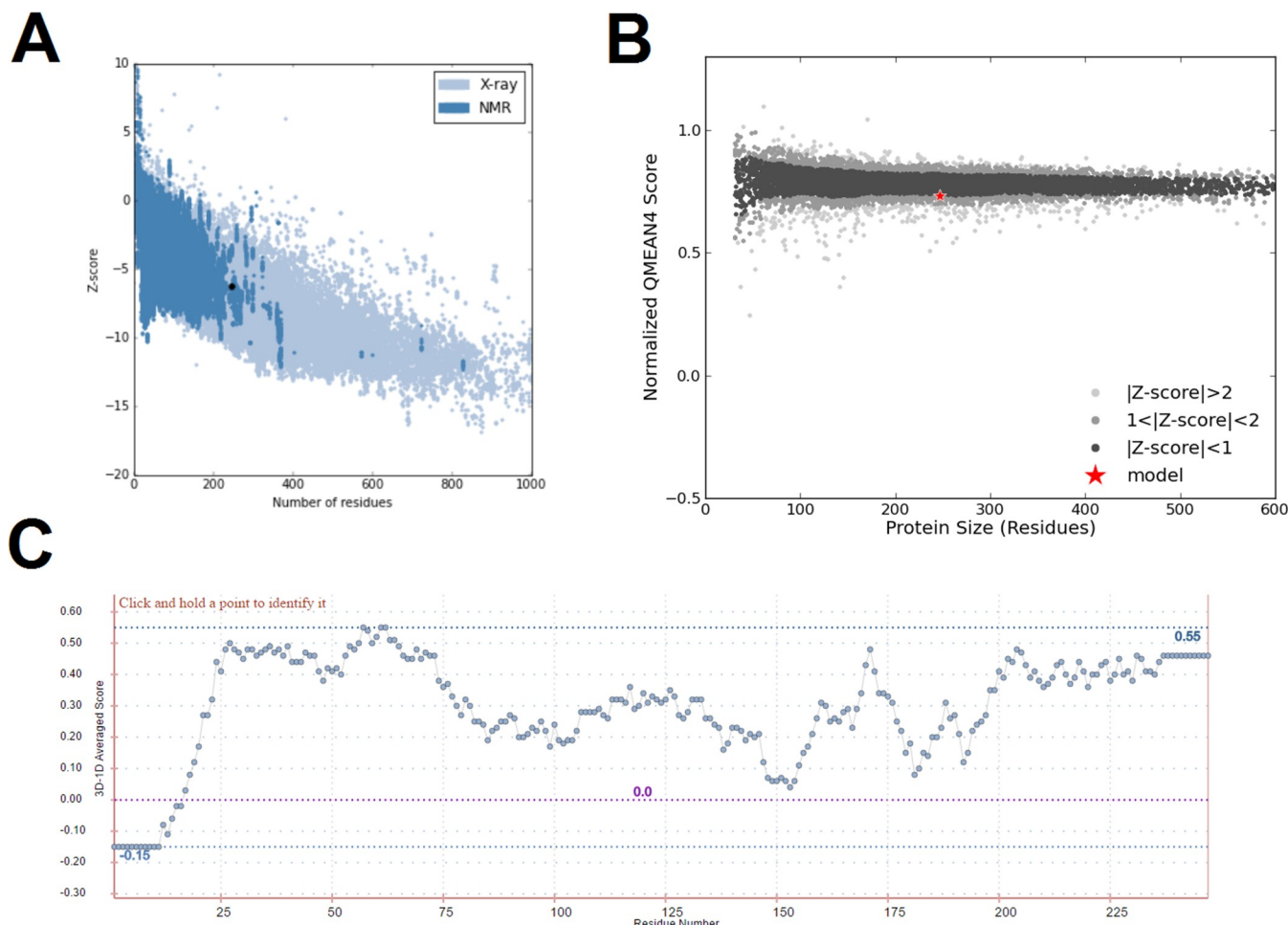


Fig 3. Validation of the *in silico* predicted model of BDNF by ProSA, QMEAN, and Verify3D. (A) Structure validation by ProSA, which shows the Z-score of the predicted model of BDNF (black dot), when compared to a non-redundant set of crystallographic structures (light blue dots) and NMR structures (dark blue dots). The *in silico* structure of BDNF presents an overall quality score comparable to that of NMR structures. (B) Structure validation by QMEAN, which shows the QMEAN-score of the predicted model of BDNF (red star), when compared to a non-redundant set of high-resolution experimental structures (gray and black dots). (C) Structure validation by Verify3D, which shows the 3D-1D score for each atom of the predicted model of BDNF. The graphic shows that 80.57% of the residues of the *in silico* structure of BDNF presented a compatibility score of 0.2 or higher, which indicates that the structure is a high-quality model according to Verify3D.

<https://doi.org/10.1371/journal.pone.0215508.g003>

With the quality assessment and the confirmation of the secondary structure prediction, the Rosetta's model was considered a high-quality model. Thus, it was selected for the subsequent analyses.

Phylogenetic analysis

ConSurf is a bioinformatics tool that applies statistical inference methods, machine learning and multiple sequence alignment to estimate the evolutionary conservation of amino acids in a protein. ConSurf then attributes a conservation score to each residue based on the phylogenetic relationship between the protein and its homologous sequences. The conservation scores are associated with a coloring scheme and projected on the protein's surface [49].

The validated model of BDNF was submitted to ConSurf, which calculated the evolutionary conservation score of each amino acid of BDNF (Fig 6). The position 66 of BDNF was classified as variable and buried.

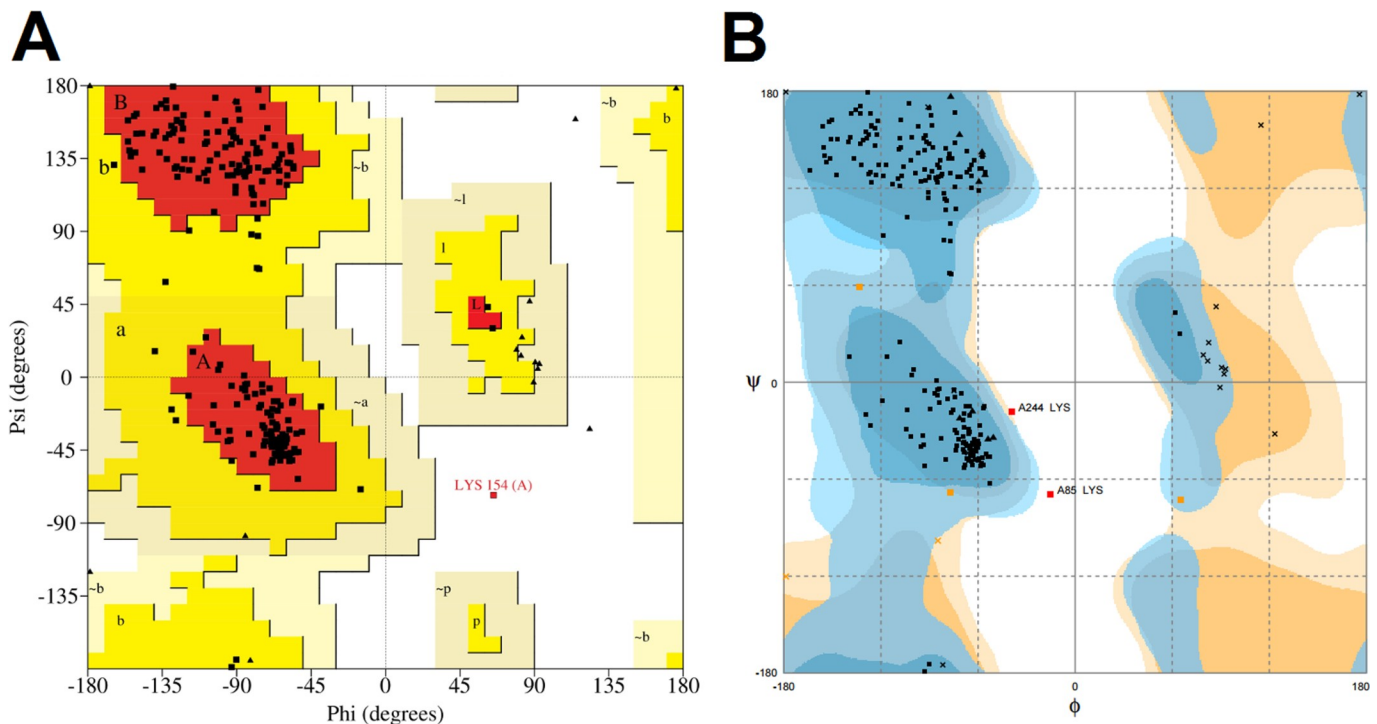


Fig 4. Validation of the *in silico* predicted model of BDNF by PROCHECK and RAMPAGE. (A) PROCHECK's Ramachandran plot shows that the *in silico* structure of BDNF. Most residues (90.8%) are located in the most favored regions, while 8.8% are in additional allowed regions, and only 0.5% in disallowed regions, configuring a high-quality model. (B) RAMPAGE's Ramachandran plot of the *in silico* structure of BDNF. This structure is also considered as a high-quality model because it shows 97.1% of its residues on favored regions, 2.0% on allowed regions, and 0.8% on not allowed regions.

<https://doi.org/10.1371/journal.pone.0215508.g004>

Molecular dynamics

MD simulations compute the time-dependent motion of a molecular system based on concepts of physics, chemistry and mathematics [60,61]. Thus, the MD approach can be used to reproduce the real behavior of a protein in its environment and to calculate its trajectory over time [20]. These simulations provide detailed information on changes in protein conformation and fluctuations that can be used to assess biochemical and structural parameters, such as flexibility and stability [60].

The impact of mutations on the structure and function of a protein can be examined using MD simulations [62]. The complete theoretical models of wild-type BDNF and its V66M variant (Fig 7) were submitted to MD simulations on GROMACS. The simulations were performed in triplicates and the obtained results were analyzed comparatively in order to understand the effects of the V66M mutation on BDNF structure and function. The means and their respective confidence intervals (0.95) were calculated for each triplicate in the RMSD, Rg and SASA.

RMSD and RMSF are common measures of structural fluctuations [61,63]. For purposes of MD, RMSD is defined as the root mean square deviation of the atoms of a structure at a given instant of the simulation relative to its initial position in the MD trajectory [63]. RMSD is therefore useful for analyzing the time-dependent motion of a given structure and for determining its spatial convergence throughout the simulation. A plateau of RMSD values indicates that the structure fluctuates around a stable average conformation. Thus it makes sense to evaluate its local fluctuations [61,63].

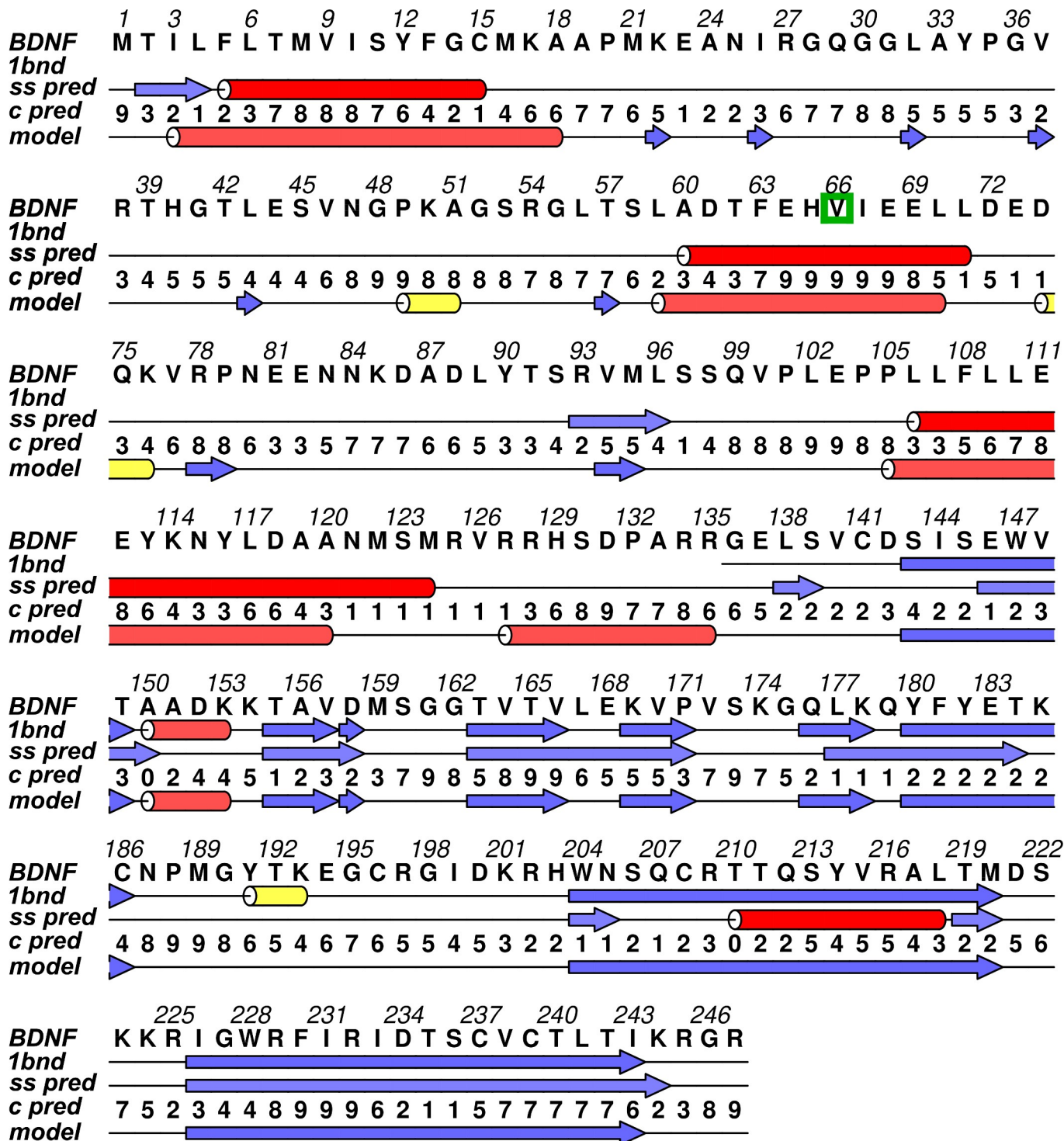


Fig 5. Secondary structure comparison between the theoretical model of BDNF, the CONCORD prediction, and the 1BND experimental fragment. The amino acid sequence of BDNF wild type is shown in the first line of the alignment, followed by the secondary structure of the 1BND fragment, the consensus secondary structure prediction by CONCORD (ss pred), the CONCORD confidence score (c pred), and the secondary structure of the theoretical model of BDNF. Red cylinders represent the α -helices, yellow cylinders represent the 3–10 helices, and blue arrows represent the β -strands.

<https://doi.org/10.1371/journal.pone.0215508.g005>

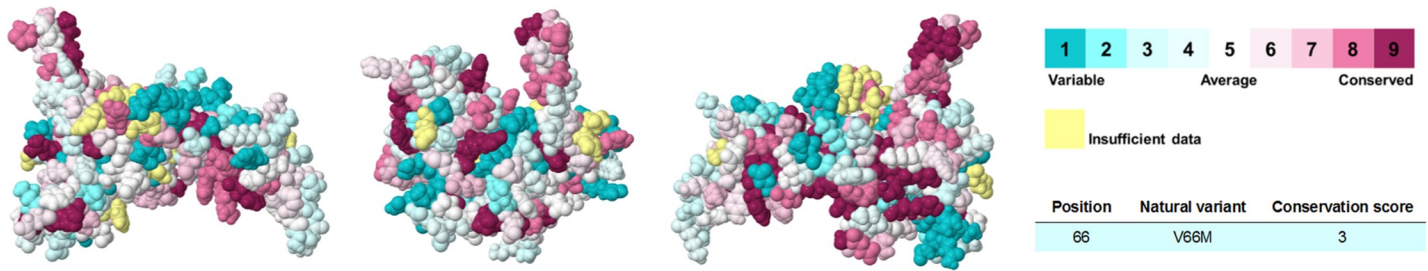


Fig 6. Evolutionary conservation analysis of BDNF. The BDNF conservation profile is shown in three different angles. The amino acid residues are represented as space-filling models and colored according to their conservation scores. The color coding bar shows the ConSurf conservation scores. The amino acid residues colored in yellow did not receive conservation scores due to insufficient data. According to ConSurf, position 66 of BDNF is variable and buried. Highly conserved positions are colored maroon, intermediately conserved residues are colored white and variable positions are colored turquoise.

<https://doi.org/10.1371/journal.pone.0215508.g006>

We analyzed the time evolution of backbone RMSD values to monitor the overall stability of each model during 200 ns MD in explicit solvent. Wild-type and V66M systems reached equilibrium in approximately 50 ns and 100 ns, respectively, and presented a steady behavior throughout the triplicates (Fig 8). Furthermore, the RMSD values of the V66M variant at the plateau (0.62 ± 0.04 nm) are similar to those of the wild-type structure (0.55 ± 0.04 nm).

The RMSD values distribution only provides information about the overall structure [64]. Thus, RMSF analysis, which assesses the deviations of an atom or group of atoms from its average position in a given structure [63,64], is often applied to obtain local information. This analysis is therefore useful to describe local flexibility, thermal stability, and heterogeneity of macromolecules [64] based on residue displacement during the MD simulation [20].

The comparison of the fluctuations between wild-type and V66M variant structures evidenced that the presence of the mutation resulted in no significant local flexibility alterations (Fig 9).

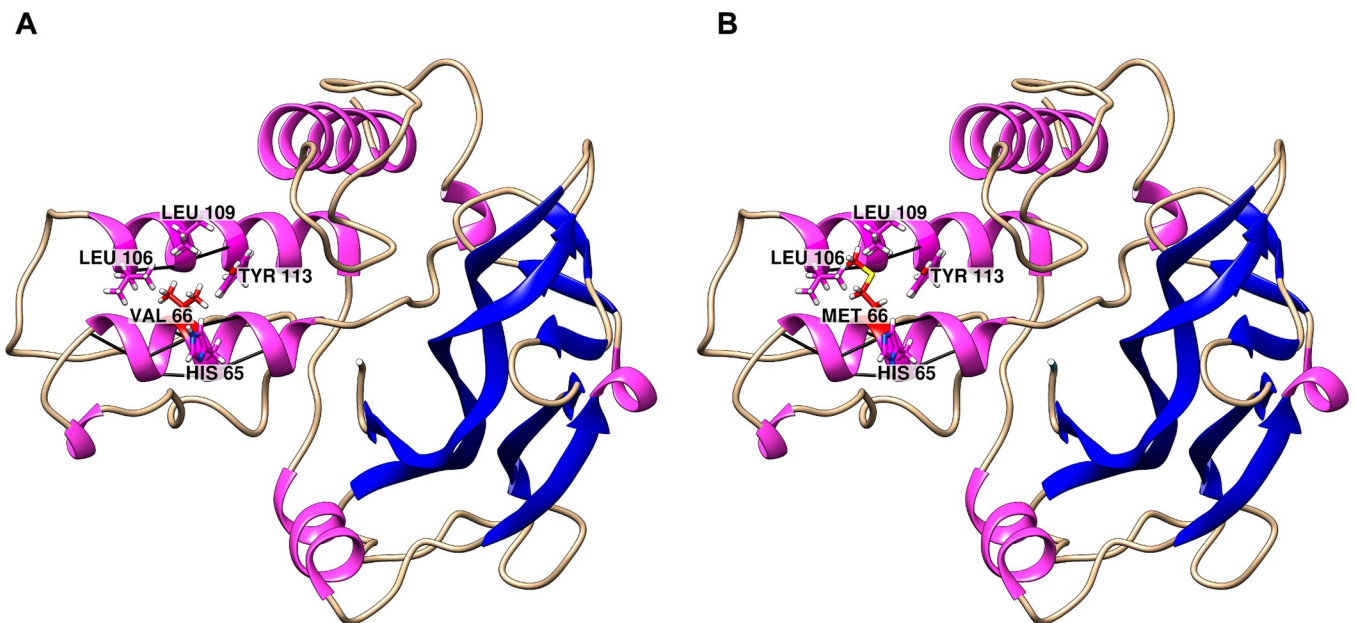


Fig 7. Complete theoretical models of wild-type BDNF and its variant V66M. Secondary structure representation of the *in silico* modeled structures of wild-type BDNF and its variant V66M. The α -helices are represented by pink ribbons, the β -strands are represented by blue arrows, and the coiled regions are represented in beige. Residues within 5 Å of val66 and met66 are shown in the sticks. Black lines represent hydrogen bonds. (A) Wild-type BDNF. (B) Variant V66M.

<https://doi.org/10.1371/journal.pone.0215508.g007>

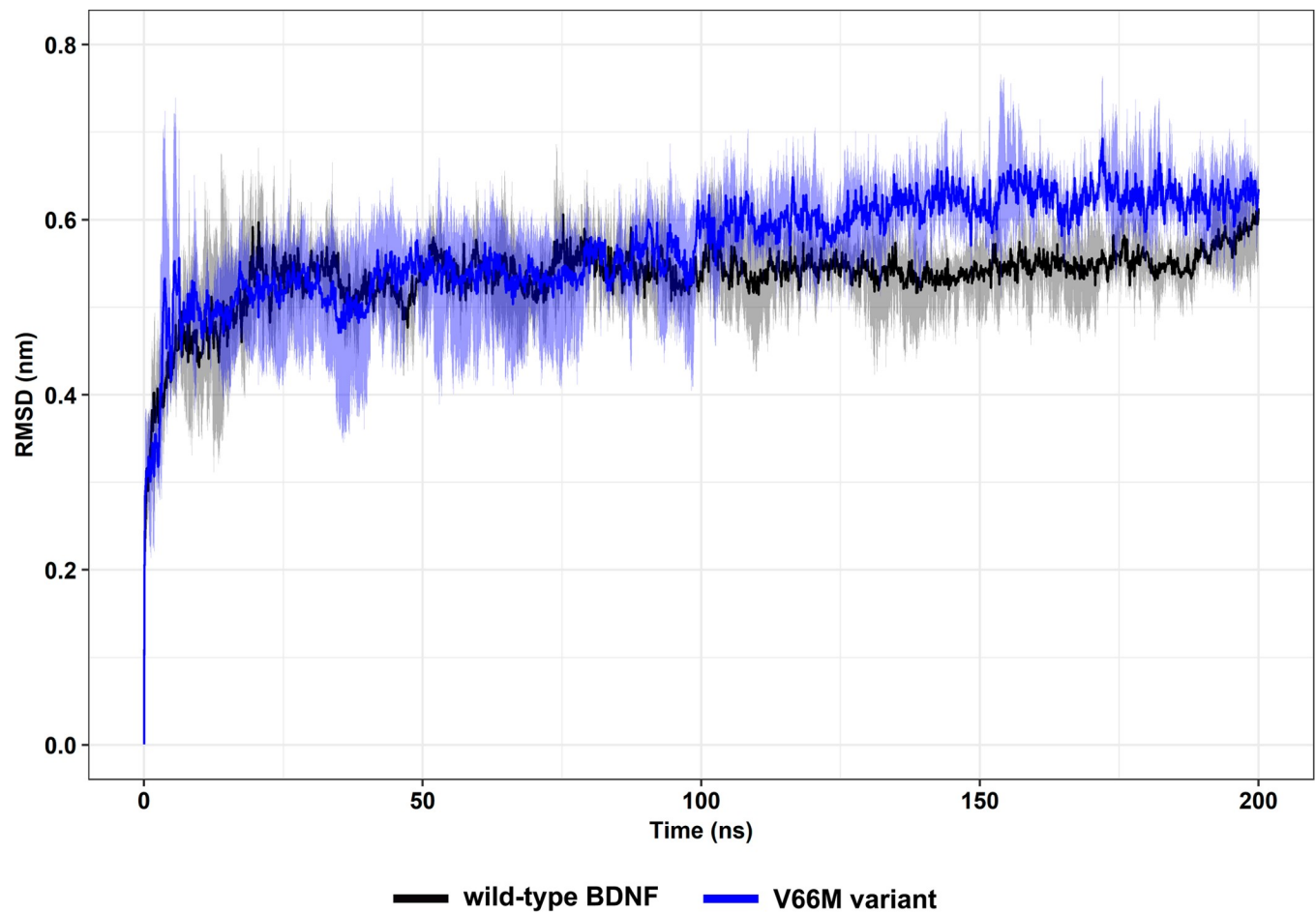


Fig 8. Backbone RMSD of wild-type BDNF and its V66M variant. RMSD of the backbone atoms of wild-type BDNF (black) and its V66M variant (blue) structures at 300 K are shown as a function of time. Mean (solid lines) and confidence interval (smooth lines) of the replicates are displayed.

<https://doi.org/10.1371/journal.pone.0215508.g008>

Structural flexibility can also be assessed during an MD simulation by analyzing the B-factor, a measure of atomic displacement due to thermal vibrations [65]. B-factor, as well as RMSF, reflects the fluctuation of an atom or a set of atoms around their average position [64,66]. B-factor is therefore used in most methods of predicting protein flexibility [65] and applied to predict protein flexibility [64].

An overview of structural mobility indicated that the flexibility of the wild-type and V66M variant of BDNF are similar (Fig 10). B-factor analysis indicated that the V66M mutation does not affect BDNF local flexibility.

The biological function of proteins is associated with their molecular motions. Therefore, a thorough understanding of protein function requires the investigation of its static structures, as well as its dynamics and molecular motions [67].

Protein dynamical mechanical properties are usually best characterized by analyzing its phase space behavior [62]. PCA, also known as essential dynamics (ED), is a statistical technique that extracts the essential motions of a protein from a set of sampled conformations using covariance or correlation matrices. Thus, PCA reduces the number of dimensions needed to describe protein dynamics [68]. The protein fluctuations are confined within the eigenvectors of the covariance matrix, which are also called principal components. Projections

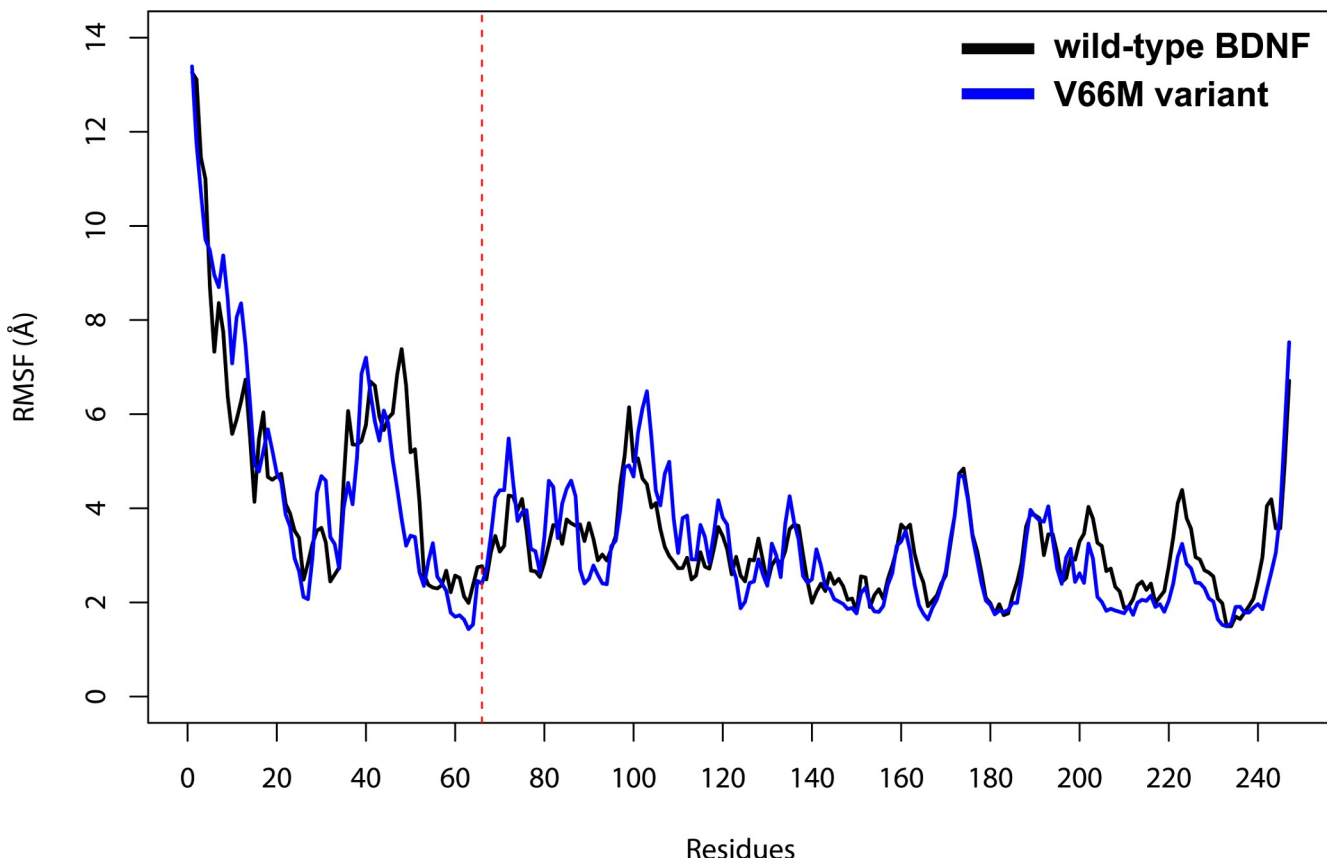


Fig 9. RMSF of wild-type BDNF and its V66M variant. RMSF of each residue of wild-type BDNF (black) and its V66M variant (blue) at 300 K are shown as a line plot. The dashed red line shows residue 66.

<https://doi.org/10.1371/journal.pone.0215508.g009>

of the protein trajectories on the eigenvectors thus describe their essential motions in phase space [62].

The ED method can be used to study the influence of residue mutations on molecular motions [67]. Therefore, we performed PCA on the snapshots obtained from the full MD trajectories to identify statistically relevant motions (essential motions) [69] of wild-type BDNF and its V66M variant in solution. The first two components (named PC1 and PC2) captured the dominant motions, accounting for 59.24% and 50.67% of the overall variance in wild-type BDNF and V66M variant, respectively. We compared the projections of the trajectories onto the subspace spanned by the first two principal components (Fig 11), as well as analyzed the RMSF contribution of each protein residue to the first two principal components (Fig 12). Overall, the variant V66M exhibited altered essential mobility when compared to the wild-type BDNF, especially at its N-terminus, suggesting that the V66M mutation could affect the BDNF essential motions.

R_g is the mass-weighted root mean square distance of a group of atoms from their common center of mass [62] and is used to describe the dimensions of proteins and other biopolymers [64]. R_g analysis, therefore, generates comprehensive information on protein compactness during an MD [70]. The overall dimensions of the wild-type and V66M variant systems presented an average R_g of 2.05 ± 0.04 nm and 2.05 ± 0.03 nm, respectively (Fig 13), suggesting that the V66M mutation does not affect the BDNF compactness.

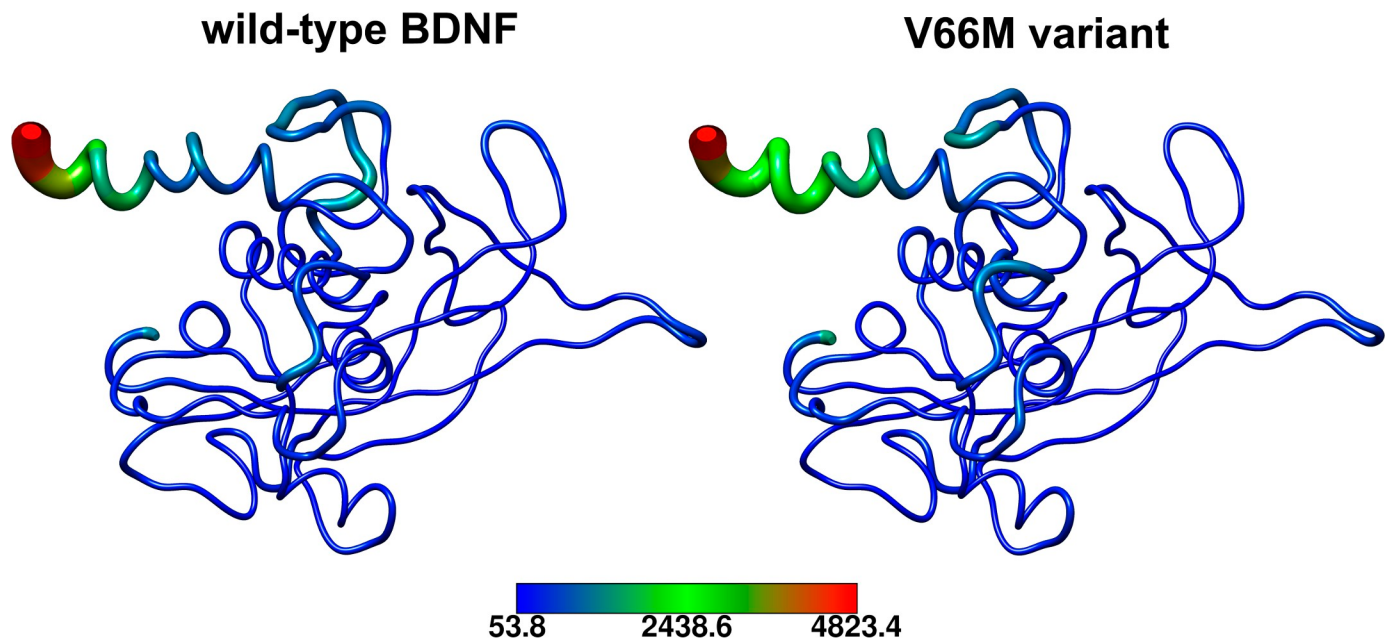


Fig 10. B-factor representation of wild-type BDNF and its V66M variant. The B-factor values of each residue of wild-type BDNF and its V66M variant expressed in a coloring-thickness scheme. Higher B-factor values are represented as red and bulky structures, while lower B-factor values are represented as dark blue and thin structures.

<https://doi.org/10.1371/journal.pone.0215508.g010>

Solvent accessible surface area (SASA) is defined as the exposed surface of a protein that can be accessed by a solvent [71,72]. Thus, SASA analysis is useful to understand the protein's ability to interact with solvents [72] and other molecules. The accessible surface area of the wild-type and V66M variant systems are similar, presenting an average SASA of $157.08 \pm 4.82 \text{ nm}^2$ and $156.25 \pm 4.31 \text{ nm}^2$, respectively (Fig 14). This analysis suggests that no significant variations in SASA were observed during the simulations.

The function of most proteins is dependent on the interaction and recognition of other molecules. In addition, much of the binding selectivity comes from the hydrogen-bonding formation between a given protein and its molecular partner [73]. The secondary structure is also a well-known factor for protein interactions [74,75], since this structural pattern may both favor or disfavor interactions, such as hydrogen-bonding [73]. We then analyzed the pattern of secondary structure (Fig 15), as well as the hydrogen-bonding formation of the residue 66 (Table 2) during the MD simulations for BDNF wild-type and its V66M variant [14].

The secondary structure analysis pointed to alterations in the pattern of secondary structure of BDNF wild-type when compared to its V66M variant, especially at the first alpha-helix of the protein, comprised between the residues 3 and 18. The second alpha-helix of BDNF, which contains the position 66 and adjacent residues, presented little alterations when compared to the wild type, particularly between 68 and 78 ns. It suggests that the V66M mutation could affect the BDNF secondary structure especially at its first alpha-helix (BDNF pre-domain), but also may affect the BDNF pro-domain (position 66 and adjacent residues) [76].

The hydrogen-bonding analysis (Table 2) indicated that the occupancy of the hydrogen bonds formed during the simulations was different for the BDNF wild-type and its V66M variant, especially regarding the hydrogen bonds formed between val66-thr62 and met66-thr62. The occupancy of the hydrogen bond formed between the main chains of val66-thr62 and met66-thr62 is respectively 92.12% and 0%.

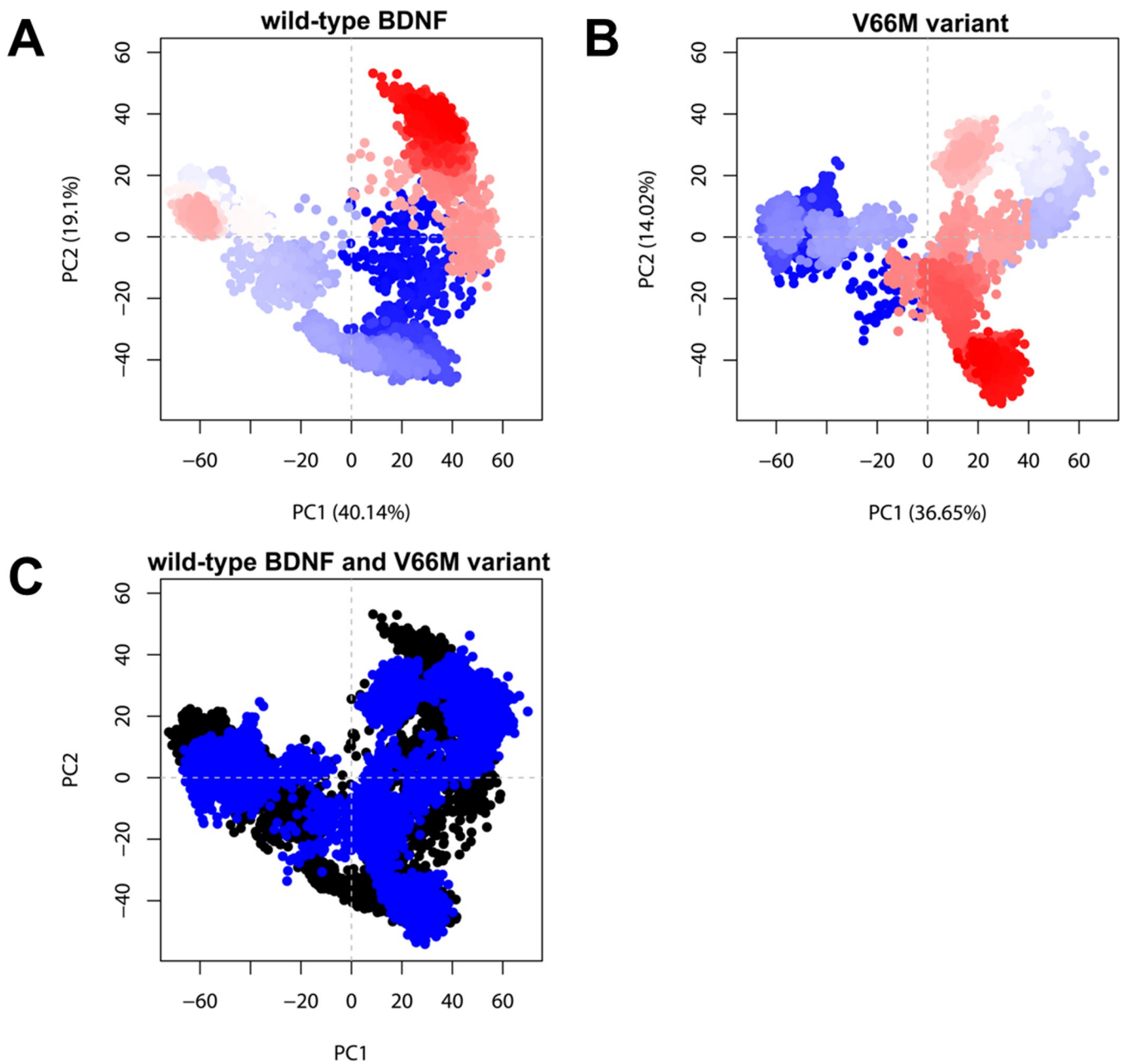


Fig 11. Principal component analysis (PCA) of wild-type BDNF and its variant V66M. The plots are showing the first two principal components (PC1 and PC2) extracted from the essential dynamics. The trajectory frames for wild-type BDNF and its variant V66M were colored from blue to red according to time evolution. (A) PCA plot of wild-type BDNF. The first two PCs account for 59.24% of the total structural variance. (B) PCA plot of variant V66M. The first two PCs account for 50.67% of the total structural variance. (C) PCA comparison between wild-type BDNF (black) and its variant V66M (blue).

<https://doi.org/10.1371/journal.pone.0215508.g011>

Discussion

BDNF plays a key role in the proliferation, maturation, and maintenance of neuronal function [8,13]. The most frequent missense mutation of BDNF in humans, V66M [13], is believed to impair protein function and distribution [14,15]. This mutation is associated with the development of psychiatric disorders [13].

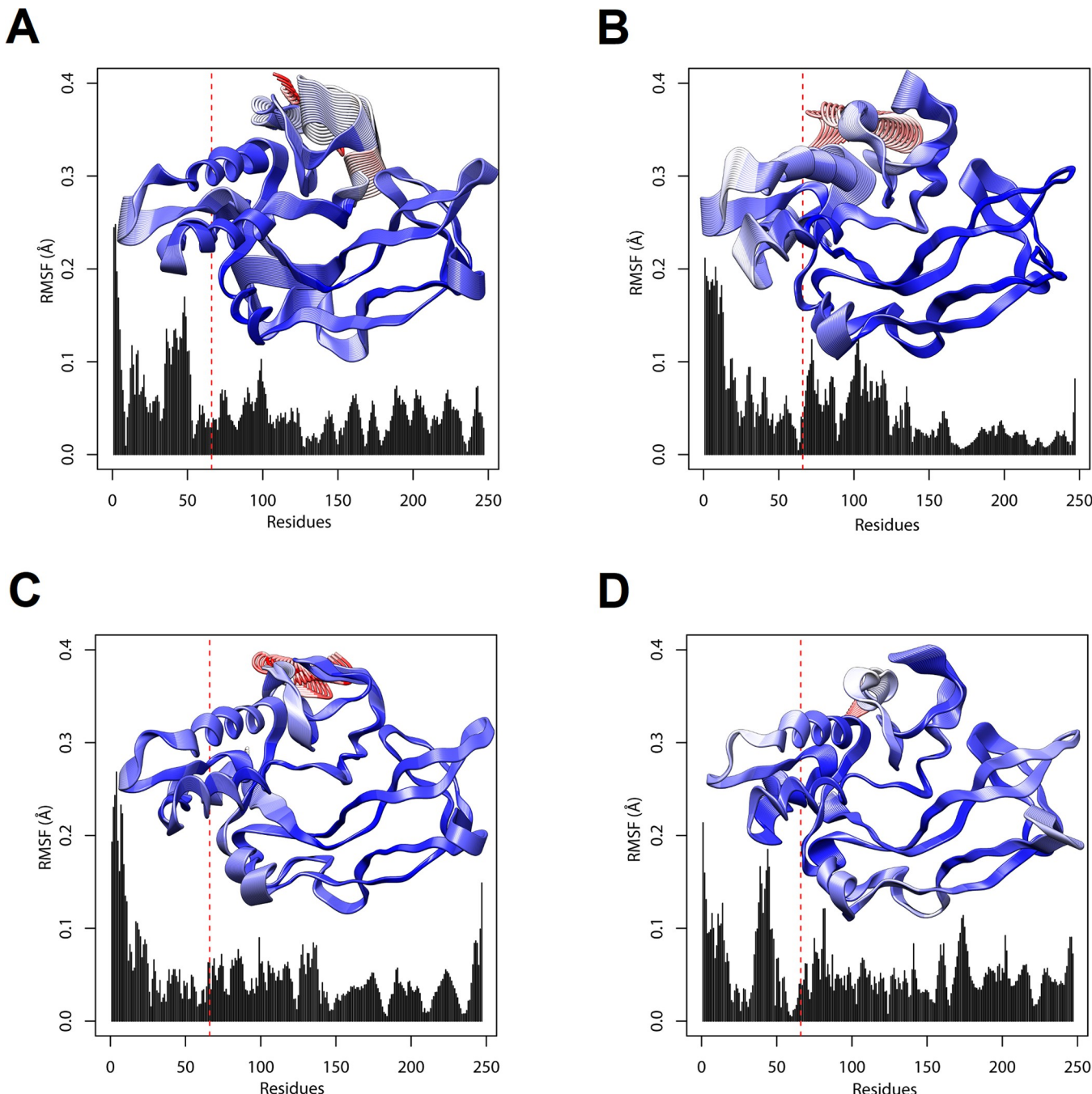


Fig 12. Visualization of the first two principal components on the structure of wild-type BDNF and its variant V66M. The RMSF contribution of each protein residue to the first two principal components (PC1 and PC2) is displayed within their respective plot and projected on the corresponding structural location. RMSF magnitude is represented by a coloring-thickness scheme, which scales from thin and blue (low fluctuations) to thick and red (large fluctuations). The dashed red lines show residue 66. (A) RMSF contribution of wild-type to PC1. (B) RMSF contribution of variant V66M to PC1. (C) RMSF contribution of wild type to PC2. (D) RMSF contribution of variant V66M to PC2.

<https://doi.org/10.1371/journal.pone.0215508.g012>

The pro-domain of BDNF, particularly the position 66 and its adjacent residues, are determinant for the intracellular sorting and activity-dependent secretion of the molecule [14]. This region also acts as a molecular chaperone to assisting the folding [77] of nascent BDNF, in

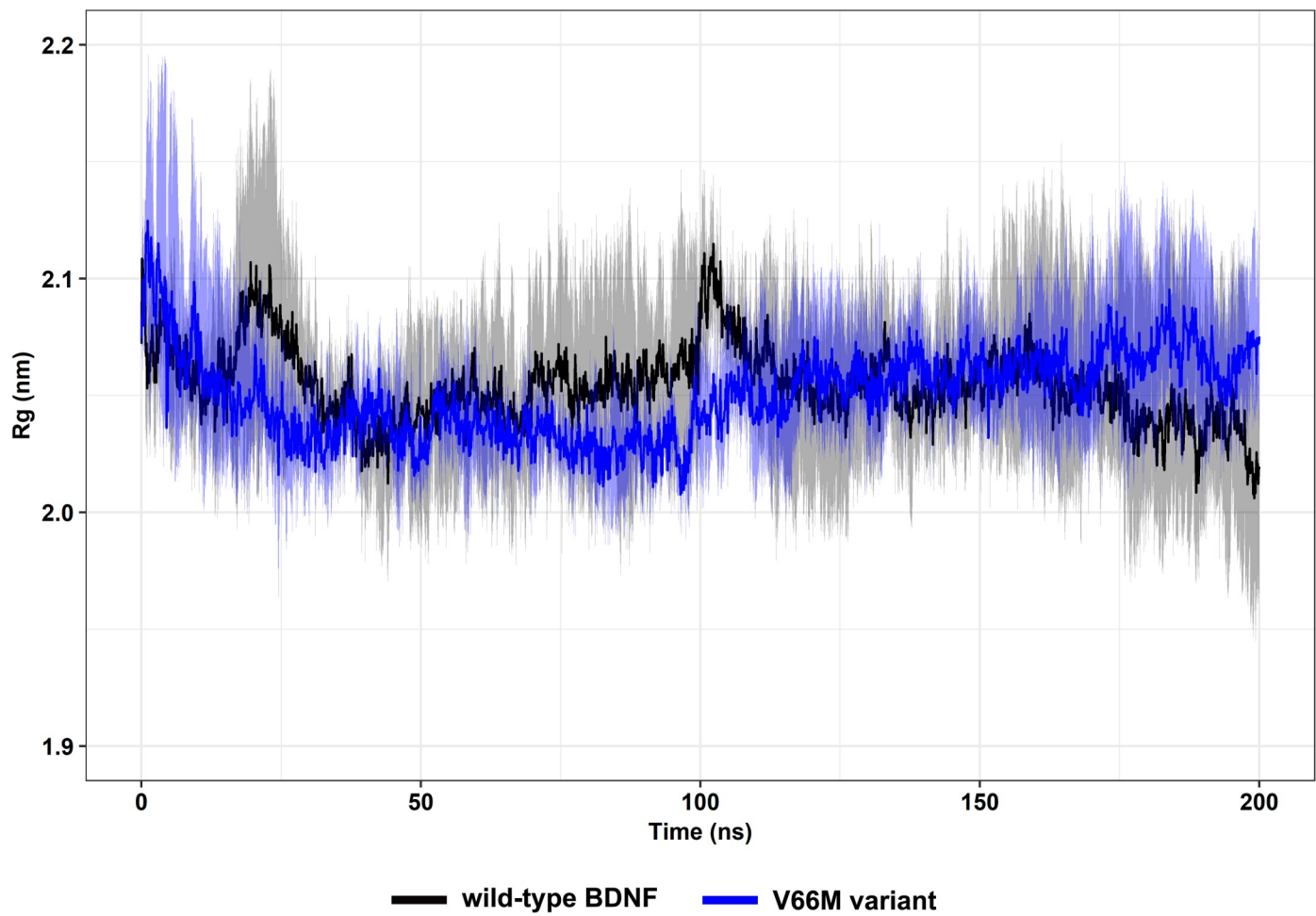


Fig 13. Rg of wild-type BDNF and its V66M variant. Rg of the C α atoms of wild-type BDNF (black) and its V66M variant (blue) at 300 K are shown as a function of time. Mean (solid lines) and confidence interval (smooth lines) of the replicates are displayed.

<https://doi.org/10.1371/journal.pone.0215508.g013>

addition to being directly involved in the proteolytic cleavage of pro-BDNF to mature-BDNF [78].

The substitution of a Valine to a Methionine at the position 66 of BDNF occurs at its N-terminal pro-region [77]. This substitution affects the intracellular sorting of BDNF [16] and reduces the amount of the protein targeted to secretory granules [11]. This pathological condition impairs the activity-dependent secretion of BDNF [79], which is the main pathway responsible for the protein release in neurons [80].

In addition to reducing BDNF secretion in neurons [77,80], the V66M mutation also impacts BDNF expression levels [81,82]. Moreover, this mutation is believed to disrupt the folding and dimerization of BDNF [16]. However, the V66M substitution does not affect the efficiency of pro-BDNF processing and, consequently, the formation of mature-BDNF [79].

The pro-domain of BDNF does not appear to participate in the protein dimerization process, since the formation of BDNF dimers depends on a cysteine knot structure linking the mature domains of each protein monomer. Importantly, this connection is maintained even after the cleavage of BDNF pro-domains [83]. However, the V66M mutation is thought to impair BDNF dimerization [16].

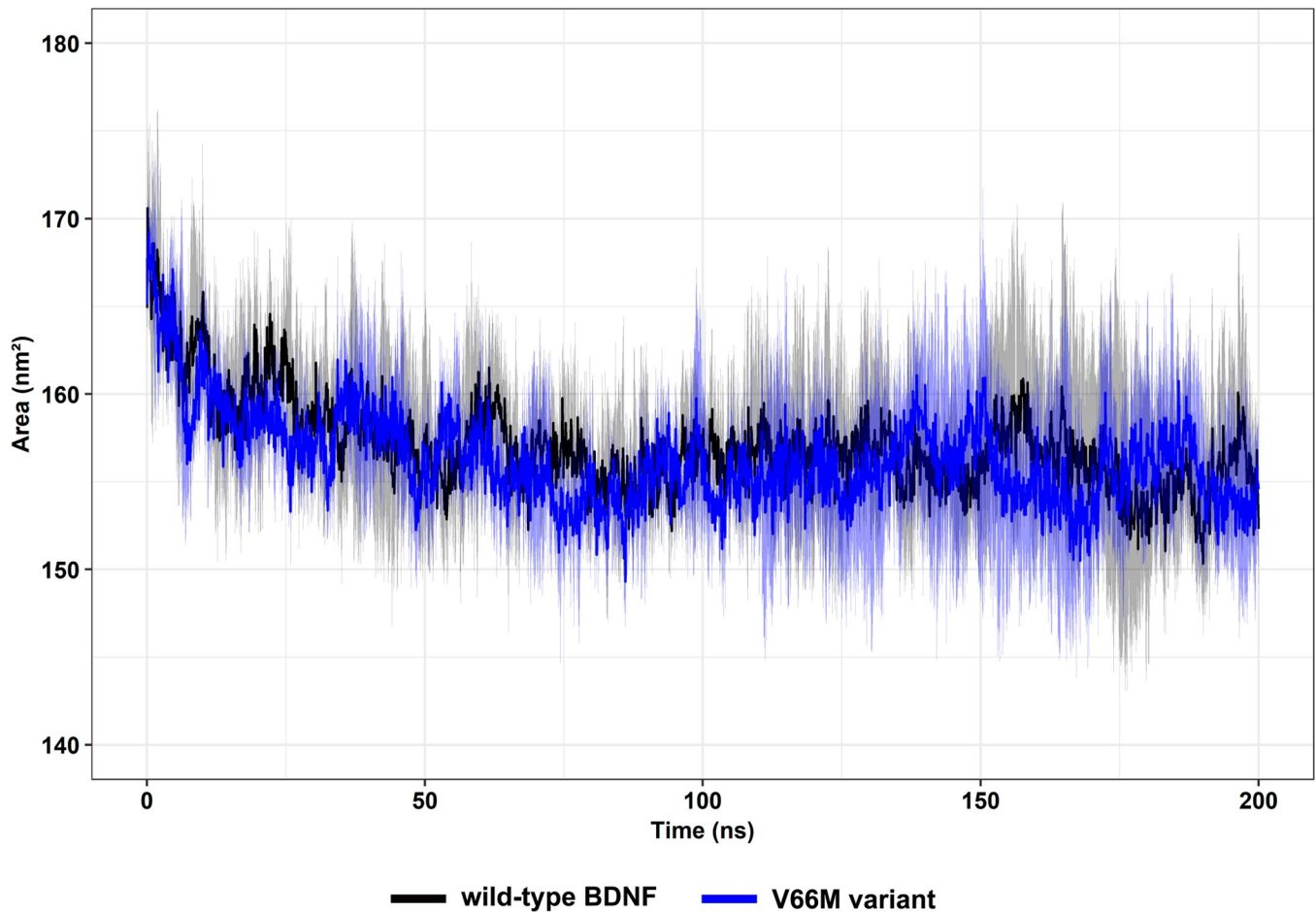


Fig 14. SASA of wild-type BDNF and its V66M variant. SASA of wild-type BDNF (black) and its V66M variant (blue) are shown as a function of time. Mean (solid lines) and confidence interval (smooth lines) of the replicates are displayed.

<https://doi.org/10.1371/journal.pone.0215508.g014>

The effects of deleterious mutations on proteins can be predicted *in silico* by computational simulations [70]. We used the PhD-SNP [28], PMut[29], PolyPhen-2 [30], SIFT [31], SNAP [32], SNPs&GO [33], VarMod [34], SNPeffec4.0 [22], and I-Mutant2.0 [35] algorithms to predict the V66M effects on the BDNF function and stability.

The V66M variant of BDNF was predicted as deleterious by SIFT and PolyPhen-2, whereas it was predicted as neutral by PhD-SNP, PMut, SNAP, SNPs&GO, and Varmod. This analysis shows little concordance amongst the functional prediction algorithms used in detecting the known deleterious potential of the V66M mutation [13,15], as only two out of the seven algorithms were able to detect it. The available methods were trained in different data sets [84] and present different strategies to predict the putative functional effects of mutations on proteins. Considering that there is no gold-standard method, it is important to use more than one algorithm to determine the deleterious potential of mutations [20,24]. The divergent results reaffirm the need of improving such methods.

The FoldX prediction indicated that the V66M mutation does not affect BDNF stability ($\Delta\Delta G = -0.04$ kcal/mol), whereas the I-Mutant prediction indicated that the V66M mutation decreases protein stability ($\Delta\Delta G = -0.49$ kcal/mol). The inconsistency between these results may occur due to the different strategies that the FoldX and I-Mutant algorithms apply to make predictions and classify mutations [35,85]. While FoldX evaluates free energy from the

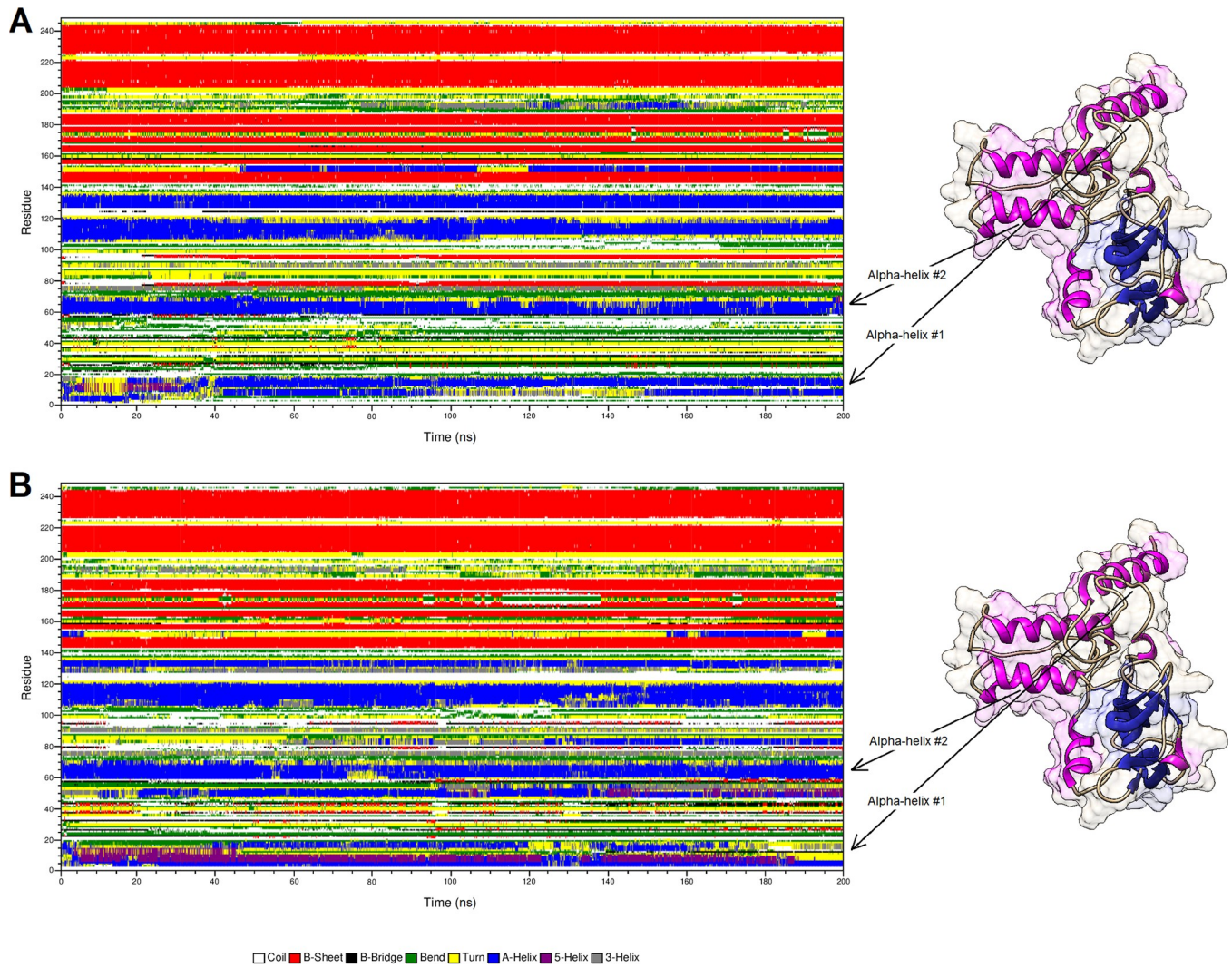


Fig 15. Secondary structure analysis of BDNF wild-type and its V66M variant. Time evolution of secondary structural elements during the MD simulations of wild-type BDNF (A) and its V66M variant (B). Coils are represented in white, β -sheets are represented in red, β -bridges are represented in black, bends are represented in green, turns are represented in yellow, α -helices are represented in blue, 5-helices are represented in purple and 3-helices are represented in gray.

<https://doi.org/10.1371/journal.pone.0215508.g015>

Table 2. Hydrogen bond occupancy of the residue 66 during the MD simulations of BDNF wild-type and its V66M variant.

Wild-type BDNF			V66M BDNF		
Donor	Acceptor	Occupancy (%)	Donor	Acceptor	Occupancy (%)
VAL66-Main-N	THR62-Main-O	92.12	MET66-Main-N	THR62-Main-O	0
VAL66-Side-CG2	THR62-Main-O	16.29	MET66-Side-CG	THR62-Main-O	7.29
LEU70-Main-N	VAL66-Main-O	24.25	LEU70-Main-N	MET66-Main-O	10.16
GLU69-Main-N	VAL66-Main-O	17.75	GLU69-Main-N	MET66-Main-O	10.59
VAL66-Main-N	PHE63-Main-O	17.95	MET66-Main-N	PHE63-Main-O	32.96

Atom pairs with less than 5% occupancy are not shown in the table.

<https://doi.org/10.1371/journal.pone.0215508.t002>

application of an empirical force field that was trained in the molecular interactions of engineered proteins [85], I-Mutant applies Support Vector Machine methods to calculate free energy based on experimentally determined structures [35]. Moreover, FoldX presented three possible classifications for the mutation effects on protein stability: does not affect protein stability ($\Delta\Delta G$ between 0.5 and -0.5 kcal/mol), decreases protein stability ($\Delta\Delta G > 0.5$) and increases protein stability ($\Delta\Delta G < -0.5$) [22], whereas for I-Mutant, there are only two possible classifications: decrease protein stability ($\Delta\Delta G < 0$) or increase protein stability ($\Delta\Delta G > 0$) [35].

The SNPeffect prediction indicated that the V66M mutation does not affect the aggregation tendency, amyloid propensity and chaperone binding tendency of BDNF.

The three-dimensional protein structure is essential for understanding the mechanisms by which proteins perform their functions [18] and the mechanisms which disease-associated mutations disrupt these functions [19]. In addition to experimental methods for determining protein structures, such as x-ray crystallography and NMR, the structure of a protein can be predicted using theoretical modeling [60]. However, considering that experimental methods of determining protein structures are expensive and time consuming [20] and that massively parallel and low-cost sequencing methods determine protein sequences at a much faster rate [19], theoretical modeling is presented as an efficient [20] and necessary approach to solving the protein structural gap [18] because it enables modeling of three-dimensional structures in a cheaper, faster, and more accurate way [20].

There are two theoretical modeling methods that are worth mentioning: comparative and *ab initio* modeling. *Ab initio* modeling predicts protein structures based on energy functions and sequence information [86], whereas comparative modeling builds three-dimensional protein models using experimentally determined structures as the template [27]. Comparative modeling is the most precise method of predicting protein structures, as it can generate models with an accuracy that is similar to that of experimental protein models [60].

BDNF has had only part of its structure experimentally determined. The available crystallographic fragments of BDNF have no structure at the position 66 and adjacent residues [17], which are located at the pro-region of the protein and are important for the release-dependent activation of BDNF [14]. Thus, we sought to develop the *in silico* complete model of BDNF and its V66M variant.

HHPred and SwissModel returned incomplete models of BDNF, whereas Rosetta, I-Tasser, RaptorX, Phyre2 and M4T returned complete models. The alignment between the modeled structures of BDNF and its crystallographic fragment (PDB ID: 1BND) by TM-align is shown in Table 1, The alignment provides two distinct values: RMSD and TM-score, which are used to evaluate the structural similarity of the submitted molecules [58]. RMSD is defined as the spatial differences between two static structures [61]. Protein size and local structural deviations are not considered in RMSD calculation. Based on this approach, the TM-align server also provides a TM-score, which is calculated from smaller portions of the structure and is normalized according to protein size, thus providing greater sensitivity in evaluating structural similarity [58]. Accurate models present TM-scores approaching 1 and $\text{RMSD} < 2.0 \text{ \AA}$ [20]. Thus, the structural alignment (Table 1) indicated the generated models are accurate. Rosetta's model (Fig 1) presented the best RMSD and TM-score values amongst the complete models and was considered the most accurate. The structural similarity between the Rosetta's model and its template structure, the experimental fragment of BDNF (PDB ID: 1BND), is shown in Fig 2.

The Rosetta's model had its stereochemical quality confirmed by PROCHECK and RAM-PAGE (Fig 4) and its 3D-1D structural compatibility confirmed by Verify3D (Fig 3C).

Moreover, the ProSa and QMEAN assessment showed that the overall quality of the Rosetta's model is comparable to that of experimental determined protein structures ([Fig 3B](#) and [3C](#)).

To further validate the modeled protein structure, we compared its secondary structure with the 1BND experimental fragment and with the CONCORD results ([Fig 5](#)). It indicates that the theoretical model of BDNF also shows high accuracy regarding its secondary structure. With the quality assessment and the confirmation of the secondary structure prediction, the theoretical model of BDNF was considered a high-quality model and selected for the subsequent analyses.

Structurally and functionally important residues of a protein are usually conserved along evolution. Thus, the biological importance of a residue can be correlated to its level of evolutionary conservation [49]. We used ConSurf to investigate the evolutionary conservation of the position 66 of BDNF. ConSurf estimates the evolutionary conservation of amino acids in a protein and attributes a conservation score to them [49].

Although the V66M mutation of BDNF is described as being associated with the development of psychiatric disorders [13,15] and occurs in a position that is determinant for the intracellular sorting and activity-dependent secretion of the protein [14], the ConSurf analysis classified position 66 of BDNF as variable and buried ([Fig 6](#)). This result could be related to the low sensitivity of the functional prediction algorithms used to predict the known deleterious potential of the V66M mutation on BDNF [13,15], as most are based on evolutionary information from the sequence to make predictions [24].

We also developed a complete theoretical model of the V66M variant of BDNF to further investigate the effects of V66M mutation on BDNF. The comparison between the *in silico* modeled structure of wild-type BDNF and its variant V66M ([Fig 7](#)) shows that the V66M substitution does not affect the side chain interactions of residue 66, as well as the possible hydrogen bonds formed. Interestingly, the hydrogen-bonding analysis we carried out ([Table 2](#)), pointed to differences in the occupancy of hydrogen bonds formed throughout the BDNF wild-type and its V66M variant simulations, indicating that the V66M mutation may affect the BDNF propensity for hydrogen bond formation at its pro-domain.

The impact of mutations on the structure and function of a protein can be thoroughly examined using MD simulations [62]. We then performed MD simulations of wild-type BDNF and its V66M variant to investigate the effects of the V66M mutation on BDNF [[70](#)]. The plateau of RMSD values, observed at both simulations ([Fig 8](#)), is similar between the BDNF wild-type and V66M variant, indicating that both structures fluctuate around a stable average conformation [61,63]. Moreover, the RMSD values of the V66M variant at the plateau are similar to those of the wild-type structure. The RMSF ([Fig 9](#)) and B-factor ([Fig 10](#)) analyses indicated no local flexibility alterations between the wild-type BDNF and its V66M variant. The changes observed in the Rg ([Fig 13](#)) and SASA ([Fig 14](#)) analyses suggested that the V66M mutation does not affect the surface-to-volume ratio of BDNF.

Since the average RMSD value of the entire simulations of wild-type BDNF ($0.55 \pm 0.04\text{nm}$ and $0.53 \pm 0.05\text{nm}$, respectively) and its variant V66M ($0.58 \pm 0.07\text{nm}$ and $0.62 \pm 0.04\text{nm}$, respectively) are similar to those at their plateaus, we then submitted the full MD trajectories of wild-type BDNF and its variant V66M to Bio3D for the PC analysis in order to capture their molecular motions for a longer time (200ns of entire simulation, instead of 100ns of plateau time).

The alterations observed in the PC analysis ([Fig 11](#)) indicated that the V66M mutation could affect the BDNF essential motions, particularly at its N-terminus ([Fig 12](#)). Considering that the biological functions of proteins are usually determined by their essential motions [67], such as binding to substrates and protein interactions [69], the alterations observed during the PC analysis, could be related to the functional impairment of BDNF upon V66M. Especially

because the BDNF pro-domain, located at its N-terminus, is determinant for the intracellular sorting, activity-dependent secretion [14], molecular folding [77], and proteolytic cleavage of BDNF [78].

Although the RMSF and B-factor analyses suggested that the V66M mutation does not affect BDNF local flexibility, the PC analysis indicated that this mutation could affect the BDNF essential dynamics. The process of applying PC analysis to a protein trajectory is also known as essential dynamics, since the essential motions of a given protein are extracted from a set of sampled conformations [68]. Certain types of internal motions, such as binding to substrates and protein interactions, allow proteins to perform their biological functions. The aim of essential dynamics, in this sense, is to determine how these movements relate to protein function and to identify the most representative degrees of freedom. The essential dynamics allows to separate a set of internal atomic movements into two subspaces: 1) the essential subspace, which contains only a few degrees of freedom [69] usually describing relevant movements to protein function [68], such as opening, closing, and flexing; 2) and the remaining subspace, which describes small irrelevant local fluctuations [69]. Thus, the PC analysis, which describes the essential movements of a protein [68], usually better characterize its mechanical behavior [70] rather than the RMSF and B-factor analysis, which describe both relevant and irrelevant local fluctuations.

The alterations observed in the secondary structure analysis (Fig 15) suggested that the V66M mutation could affect the BDNF secondary structure at its N-terminus, especially at the BDNF first alpha-helix (pre-domain). The BDNF pre-domain leads the newly-generated protein to the endoplasmic reticulum, where it is cleaved to pro-BDNF. This constitutes a crucial step in the processing of BDNF [87]. The secondary structure analysis also pointed to little alterations at the BDNF pro-domain, which is crucial for BDNF functionality [14,77,78]. Thus, considering that the function of most proteins is guided by interactions with other molecules and, consequently, dependent on hydrogen-bonding [73] and secondary structure formation [73–75], the alterations observed in the secondary structure (Fig 15) and hydrogen-bonding analysis (Table 2) further indicate that the V66M mutation may affect BDNF functional interactions particularly at its pre and pro-domain.

The MD analyses suggested that the V66M mutation does not affect the BDNF local flexibility and surface-to-volume ratio, but could affect the BDNF essential motions, particularly at its N-terminus. The MD analyses also suggested that the V66M mutation could affect the BDNF hydrogen-bonding at its pro-domain, as well as its secondary structure at the N-terminus (pre and pro-domain). Thus, considering that hydrogen-bonding, secondary structure formation and essential dynamics are determinant for protein interactions and, consequently, protein function [69,73–75]; the alterations observed throughout the MD simulations may be associated with the functional impairment of BDNF upon this mutation [67], as well as its involvement in psychiatric disorders [8,13]. Especially because these alterations may impact BDNF effective interactions at the pre and pro-domain, which are fundamental for the processing [87], intracellular sorting, activity-dependent secretion [14], molecular folding [77], and proteolytic cleavage of BDNF [78].

Conclusions

Computational (*in silico*) approaches are efficient and necessary to predict protein structures and study disease-associated mutations. This work provided an accurate and complete model of BDNF *in silico*. Stability and functional predictions pointed to the low accuracy of the algorithms used in predicting the known deleterious potential of the V66M mutation and showed the importance of combining more than one method to predict the effects of non-synonymous

mutations. Phylogenetic analysis indicated that position 66 of BDNF is not conserved; however, it is fundamental for the intracellular sorting and activity-dependent secretion of the protein. The conservation degree of position 66 of BDNF could also be related to the low accuracy of the algorithms used in predicting the known deleterious potential of the V66M mutation, since most of them are based on evolutionary information to make predictions.

Furthermore, MD analyses indicated that the V66M mutation does not affect the BDNF flexibility and surface-to-volume ratio, but affects the BDNF essential motions, hydrogen-bonding and secondary structure formation, particularly at its N-terminus. Thus, considering that these parameters are determinant for protein interactions and, consequently, protein function; the alterations observed during the MD analyses may be related to the functional impairment of BDNF upon V66M mutation, as well as its involvement in psychiatric disorders. Especially because the BDNF N-terminus, which contains its pre and pro-region, is crucial for its activity and distribution.

Acknowledgments

We would like to thank the financial support provided by Fundação Carlos Chagas Filho de Amparo à Pesquisa do Estado do Rio de Janeiro (FAPERJ), Coordenação de Aperfeiçoamento de Pessoal de Nível Superior (CAPES), Financiadora de Estudos e Projetos (FINEP), and Conselho Nacional de Desenvolvimento Científico e Tecnológico (CNPq). We gratefully acknowledge the support of NVIDIA Corporation with their donation of the Titan X Pascal GPU used for this study. We also thank Natasha Jorge for helping us reviewing the manuscript.

Author Contributions

Conceptualization: Clara Carolina Silva De Oliveira, Gabriel Rodrigues Coutinho Pereira, Joelma Freire De Mesquita.

Data curation: Gabriel Rodrigues Coutinho Pereira.

Formal analysis: Clara Carolina Silva De Oliveira, Gabriel Rodrigues Coutinho Pereira, Deborah Antunes.

Funding acquisition: Joelma Freire De Mesquita.

Investigation: Clara Carolina Silva De Oliveira, Gabriel Rodrigues Coutinho Pereira, Jamile Yvis Santos De Alcantara.

Methodology: Clara Carolina Silva De Oliveira, Gabriel Rodrigues Coutinho Pereira, Jamile Yvis Santos De Alcantara, Deborah Antunes, Ernesto Raul Caffarena.

Project administration: Joelma Freire De Mesquita.

Resources: Joelma Freire De Mesquita.

Software: Ernesto Raul Caffarena.

Supervision: Joelma Freire De Mesquita.

Validation: Gabriel Rodrigues Coutinho Pereira, Deborah Antunes.

Writing – original draft: Clara Carolina Silva De Oliveira, Gabriel Rodrigues Coutinho Pereira, Deborah Antunes, Ernesto Raul Caffarena.

Writing – review & editing: Joelma Freire De Mesquita.

References

1. Martins-De-Souza D. Biomarkers for psychiatric disorders: Where are we standing? *Dis Markers*. 2013; 35: 1–2. <https://doi.org/10.1155/2013/321071> PMID: 24167343
2. Roy M, Tapadia MG, Joshi S, Koch B. Molecular and genetic basis of depression. *J Genet*. 2014; 93: 879–892. PMID: 25572252
3. Trautmann S, Rehm J, Wittchen H-U. The economic costs of mental disorders. *EMBO Rep*. 2016; 17: 1245–1249. <https://doi.org/10.1525/embr.201642951> PMID: 27491723
4. Walker ER, McGee RE, Druss BG. Mortality in Mental Disorders and Global Disease Burden Implications. *JAMA Psychiatry*. 2015; 72: 334–341. <https://doi.org/10.1001/jamapsychiatry.2014.2502> PMID: 25671328
5. Safran JJ, Schwartz D, Rineer J, Weiner JP, Wong A, Schreiber D. Does the Presence of a Major Psychiatric Disorder Affect Tolerance and Outcomes in Men With Prostate Cancer Receiving Radiation Therapy? *Am J Mens Health*. 2015; 1–8. <https://doi.org/10.1177/1557988315610626> PMID: 26487340
6. Chesney E, Goodwin GM, Fazel S. Risks of all-cause and suicide mortality in mental disorders: A meta-review. *World Psychiatry*. 2014; 13: 153–160. <https://doi.org/10.1002/wps.20128> PMID: 24890068
7. Deacon BJ. The biomedical model of mental disorder: A critical analysis of its validity, utility, and effects on psychotherapy research. *Clin Psychol Rev*. Elsevier Ltd; 2013; 33: 846–861. <https://doi.org/10.1016/j.cpr.2012.09.007> PMID: 23664634
8. Serra-Millàs M. Are the changes in the peripheral brain-derived neurotrophic factor levels due to platelet activation? *World J Psychiatry*. 2016; 6: 84–101. <https://doi.org/10.5498/wjp.v6.i1.84> PMID: 27014600
9. Bateman A, Martin MJ, O'Donovan C, Magrane M, Alpi E, Antunes R, et al. UniProt: The universal protein knowledgebase. *Nucleic Acids Res*. 2017; 45: D158–D169. <https://doi.org/10.1093/nar/gkw1099> PMID: 27899622
10. Wheeler DL, Chappay C, Lash AE, Leipe DD, Madden TL, Schuler GD, et al. Database resources of the National Center for Biotechnology Information. *Nucleic Acids Res*. 2000; 28: 10–4. gkd055 [pii] ET —1999/12/11 PMID: 10592169
11. Leßmann V, Brigadski T. Mechanisms, locations, and kinetics of synaptic BDNF secretion: An update. *Neurosci Res*. 2009; 65: 11–22. <https://doi.org/10.1016/j.neures.2009.06.004> PMID: 19523993
12. Lessmann V, Gottmann K, Malcangio M. Neurotrophin secretion: Current facts and future prospects. *Prog Neurobiol*. 2003; 69: 341–374. [https://doi.org/10.1016/S0301-0082\(03\)00019-4](https://doi.org/10.1016/S0301-0082(03)00019-4) PMID: 12787574
13. Autry AE, Monteggia LM. Brain-derived neurotrophic factor and neuropsychiatric disorders. *Pharmacol Rev*. 2012; 64: 238–258. <https://doi.org/10.1124/pr.111.005108> PMID: 22407616
14. Egan MF, Kojima M, Callicott JH, Goldberg TE, Kolachana BS, Bertolino A, et al. The BDNF val66met polymorphism affects activity-dependent secretion of BDNF and human memory and hippocampal function. *Cell*. 2003; 112: 257–269. [https://doi.org/10.1016/S0092-8674\(03\)00035-7](https://doi.org/10.1016/S0092-8674(03)00035-7) PMID: 12553913
15. Williams AJ, Umemori H. The best-laid plans go oft awry: Synaptogenic growth factor signaling in neuropsychiatric disease. *Front Synaptic Neurosci*. 2014; 6: 1–20. <https://doi.org/10.3389/fnsyn.2014.00001>
16. Zeev B, Ben-Babbington A, Ho G, Leonard H, De Klerk N, Gak E, et al. The common BDNF polymorphism may be a modifier of disease severity in Rett syndrome. *Neurology*. 2009; 72: 1242–1247. <https://doi.org/10.1212/01.wnl.0000345664.72220.6a> PMID: 19349604
17. Rose PW, Prlić A, Altunkaya A, Bi C, Bradley AR, Christie CH, et al. The RCSB protein data bank: Integrative view of protein, gene and 3D structural information. *Nucleic Acids Res*. 2017; 45: D271–D281. <https://doi.org/10.1093/nar/gkw1000> PMID: 27794042
18. Dorn M, e Silva MB, Buriol LS, Lamb LC. Three-dimensional protein structure prediction: Methods and computational strategies. *Comput Biol Chem*. 2014; 53: 251–276. <https://doi.org/10.1016/j.combiolchem.2014.10.001> PMID: 25462334
19. Gao M, Zhou H, Skolnick J. Insights into disease-associated mutations in the human proteome through protein structural analysis. *Structure*. 2016; 23: 1362–1369. <https://doi.org/10.1038/nbt.3121> ChIP-nexus
20. Krebs BB, De Mesquita JF. Amyotrophic Lateral Sclerosis Type 20—In Silico Analysis and Molecular Dynamics Simulation of hnRNPA1. Xia XG, editor. PLoS One. Public Library of Science; 2016; 11: e0158939. <https://doi.org/10.1371/journal.pone.0158939> PMID: 27414033
21. Ferrer-Costa C, Orozco M, de la Cruz X. Characterization of disease-associated single amino acid polymorphisms in terms of sequence and structure properties. *J Mol Biol*. 2002; 315: 771–786. <https://doi.org/10.1006/jmbi.2001.5255> [pii] PMID: 11812146

22. De Baets G, Van Durme J, Reumers J, Maurer-Stroh S, Vanhee P, Dopazo J, et al. SNPeffect 4.0: Online prediction of molecular and structural effects of protein-coding variants. Nucleic Acids Res. 2012; 40: D935–D939. <https://doi.org/10.1093/nar/gkr996> PMID: 22075996
23. De Carvalho MDC, De Mesquita JF. Structural Modeling and In Silico Analysis of Human Superoxide Dismutase 2. PLoS One. 2013; 8. <https://doi.org/10.1371/journal.pone.0065558> PMID: 23785434
24. Moreira LGA, Pereira LC, Drummond PR, De Mesquita JF, Andersen P, Phukan J, et al. Structural and Functional Analysis of Human SOD1 in Amyotrophic Lateral Sclerosis. Le W, editor. PLoS One. Public Library of Science; 2013; 8: e81979. <https://doi.org/10.1371/journal.pone.0081979> PMID: 24312616
25. Pereira GRC, Da Silva ANR, Do Nascimento SS, De Mesquita JF. In silico analysis and molecular dynamics simulation of human superoxide dismutase 3 (SOD3) genetic variants. J Cell Biochem. 2018; Sep: 1–16. <https://doi.org/10.1002/jcb.27636> PMID: 30206983
26. Amberger JS, Hamosh A. in Man (OMIM): A Knowledgebase of Human Genes and Genetic Phenotypes. Curr Protoc Bioinforma. 2017; 58. <https://doi.org/10.1002/cpb1.27> PMID: 28654725
27. Webb B, Sali A. Comparative Protein Structure Modeling Using MODELLER. Curr Protoc Bioinforma. 2016;54. <https://doi.org/10.1002/cpb1.3.Comparative>
28. Capriotti E, Calabrese R, Casadio R. Predicting the insurgence of human genetic diseases associated to single point protein mutations with support vector machines and evolutionary information. Bioinformatics. 2006; 22: 2729–2734. <https://doi.org/10.1093/bioinformatics/btl423> PMID: 16895930
29. López-Ferrando V, Gazzo A, De La Cruz X, Orozco M, Gelpí JL. PMut: A web-based tool for the annotation of pathological variants on proteins, 2017 update. Nucleic Acids Res. 2017; 45: W222–W228. <https://doi.org/10.1093/nar/gkx313> PMID: 28453649
30. Adzhubei I, Jordan DM, Sunyaev SR. Predicting Functional Effect of Human Missense Mutations Using PolyPhen-2. Curr Protoc Hum Genet. 2013;7: Unit7.20. <https://doi.org/10.1002/0471142905.hg0720s76.Predicting>
31. Vaser R, Adusumalli S, Leng SN, Sikic M, Ng PC. SIFT missense predictions for genomes. Nat Protoc. Nature Publishing Group; 2015; 4: 1073–1081. <https://doi.org/10.1038/nprot.2015.123>
32. Bromberg Y, Rost B. SNAP: Predict effect of non-synonymous polymorphisms on function. Nucleic Acids Res. 2007; 35: 3823–3835. <https://doi.org/10.1093/nar/gkm238> PMID: 17526529
33. Capriotti E, Calabrese R, Fariselli P, Martelli PL, Altman RB, Casadio R. WS-SNPs&GO: a web server for predicting the deleterious effect of human protein variants using functional annotation. BMC Genomics. BioMed Central Ltd; 2013; 14: S6. <https://doi.org/10.1186/1471-2164-14-S3-S6> PMID: 23819482
34. Pappalardo M, Wass MN. VarMod: Modelling the functional effects of non-synonymous variants. Nucleic Acids Res. 2014; 42: W331–W336. <https://doi.org/10.1093/nar/gku483> PMID: 24906884
35. Capriotti E, Fariselli P, Casadio R. I-Mutant2.0: Predicting stability changes upon mutation from the protein sequence or structure. Nucleic Acids Res. 2005; 33: W306–W310. <https://doi.org/10.1093/nar/gki375> PMID: 15980478
36. Söding J, Biegert A, Lupas AN. The HHpred interactive server for protein homology detection and structure prediction. Nucleic Acids Res. 2005; 33: W244–W248. <https://doi.org/10.1093/nar/gki408> PMID: 15980461
37. Rykunov D, Steinberger E, Madrid-Aliste CJ, Fiser A. Improved scoring function for comparative modeling using the M4T method. J Struct Funct Genomics. 2009; 10: 95–99. <https://doi.org/10.1007/s10969-008-9044-9> PMID: 18985440
38. Källberg M, Wang H, Wang S, Peng J, Wang Z, Lu H, et al. Template-based protein structure modeling using the RaptorX web server. Nat Protoc. 2016; 7: 1511–1522. <https://doi.org/10.1038/nprot.2012.085.Template-based>
39. Biasini M, Bienert S, Waterhouse A, Arnold K, Studer G, Schmidt T, et al. SWISS-MODEL: Modelling protein tertiary and quaternary structure using evolutionary information. Nucleic Acids Res. 2014; 42: 252–258. <https://doi.org/10.1093/nar/gku340> PMID: 24782522
40. Ovchinnikov S, Park H, Kim DE, Dimaio F, Baker D. Protein structure prediction using Rosetta in CASP12. Proteins Struct Funct Bioinforma. 2017; <https://doi.org/10.1002/prot.25390> PMID: 28940798
41. Zhang C, Mortuza SM, He B, Wang Y, Zhang Y. Template-based and free modeling of I-TASSER and QUARK pipelines using predicted contact maps in CASP12. Proteins Struct Funct Bioinforma. 2017; <https://doi.org/10.1002/prot>
42. Kelley LA, Mezulis S, Yates C, Wass M, Sternberg M. The Phyre2 web portal for protein modelling, prediction, and analysis. Nat Protoc. Nature Publishing Group; 2015; 10: 845–858. <https://doi.org/10.1038/nprot.2015.053> PMID: 25950237
43. Laskowski R a, Rullmann J a, MacArthur MW, Kaptein R, Thornton JM. AQUA and PROCHECK-NMR: programs for checking the quality of protein structures solved by NMR. J Biomol NMR. 1996; 8: 477–486. <https://doi.org/10.1007/BF00228148> PMID: 9008363

44. Wiederstein M, Sippl MJ. ProSA-web: Interactive web service for the recognition of errors in three-dimensional structures of proteins. *Nucleic Acids Res.* 2007; 35: 407–410. <https://doi.org/10.1093/nar/gkm290> PMID: 17517781
45. Eisenberg D, Lüthy R, Bowie JU. VERIFY3D: assessment of protein models with three-dimensional profiles. *Methods Enzymol.* 1997; 277: 396–404. Available: <http://www.ncbi.nlm.nih.gov/pubmed/9379925> PMID: 9379925
46. Wang W, Xia M, Chen J, Deng F, Yuan R, Zhang X, et al. Data set for phylogenetic tree and RAMPAGE Ramachandran plot analysis of SODs in *Gossypium raimondii* and *G. arboreum*. *Data Br.* Elsevier; 2016; 9: 345–348. <https://doi.org/10.1016/j.dib.2016.05.025> PMID: 27672674
47. Benkert P, Künzli M, Schwede T. QMEAN server for protein model quality estimation. *Nucleic Acids Res.* 2009; 37: W510–W514. <https://doi.org/10.1093/nar/gkp322> PMID: 19429685
48. WEI Y, THOMPSON J, FLOUDAS CA. CONCORD: a consensus method for protein secondary structure prediction via mixed integer linear optimization. *Proc R Soc A.* 2012; 468: 831–850. <https://doi.org/10.1098/rspa.2011.0514>
49. Ashkenazy H, Abadi S, Martz E, Chay O, Mayrose I, Pupko T, et al. ConSurf 2016: an improved methodology to estimate and visualize evolutionary conservation in macromolecules. *Nucleic Acids Res.* 2016; 44: 344–350. <https://doi.org/10.1093/nar/gkw408> PMID: 27166375
50. Gajula KS, Huwe PJ, Mo CY, Crawford DJ, Stivers JT, Radhakrishnan R, et al. High-throughput mutagenesis reveals functional determinants for DNA targeting by activation-induced deaminase. *Nucleic Acids Res.* 2014; 42: 9964–9975. <https://doi.org/10.1093/nar/gku689> PMID: 25064858
51. Humphrey W, Dalke A, Schulten K. VMD: visual molecular dynamics. *J Mol Graph.* 1996; 14: 33–8, 27–8. Available: <http://www.ncbi.nlm.nih.gov/pubmed/8744570> PMID: 8744570
52. Abraham MJ, Murtola T, Schulz R, Páll S, Smith JC, Hess B, et al. GROMACS: High performance molecular simulations through multi-level parallelism from laptops to supercomputers. *SoftwareX.* 2015; 1: 19–25. <https://doi.org/10.1016/j.softx.2015.06.001>
53. Lindorff-Larsen K, Piana S, Palmo K, Maragakis P, Klepeis JL, Dror RO, et al. Improved side-chain torsion potentials for the Amber ff99SB protein force field. *Proteins Struct Funct Bioinforma.* 2010; 78: 1950–1958. <https://doi.org/10.1002/prot.22711> PMID: 20408171
54. Hess B. P-LINCS: A Parallel Linear Constraint Solver for Molecular Simulation. *J Chem Theory Comput.* 2008; 4: 116–22. <https://doi.org/10.1021/ct700200b> PMID: 26619985
55. Essmann U, Perera L, Berkowitz ML, Darden T, Lee H, Pedersen LG. A smooth particle mesh Ewald method. *J Chem Phys.* AIP Publishing; 1995; 103: 8577. <https://doi.org/10.1063/1.470117>
56. Wickham H. *Ggplot2: elegant graphics for data analysis.* Springer; 2009.
57. Grant BJ, Rodrigues APC, ElSawy KM, McCammon JA, Caves LSD. Bio3d: An R package for the comparative analysis of protein structures. *Bioinformatics.* 2006; 22: 2695–2696. <https://doi.org/10.1093/bioinformatics/btl461> PMID: 16940322
58. Zhang Y, Skolnick J. TM-align: A protein structure alignment algorithm based on the TM-score. *Nucleic Acids Res.* 2005; 33: 2302–2309. <https://doi.org/10.1093/nar/gki524> PMID: 15849316
59. Bond CS, Schüttelkopf AW. ALINE: A WYSIWYG protein-sequence alignment editor for publication-quality alignments. *Acta Crystallogr Sect D Biol Crystallogr.* 2009; 65: 510–512. <https://doi.org/10.1107/S0907444909007835> PMID: 19390156
60. Khan FI, Wei DQ, Gu KR, Hassan MI, Tabrez S. Current updates on computer aided protein modeling and designing. *Int J Biol Macromol.* Elsevier B.V.; 2016; 85: 48–62. <https://doi.org/10.1016/j.ijbiomac.2015.12.072> PMID: 26730484
61. Knapp B, Frantl S, Cibena M, Schreiner W, Bauer P. Is an intuitive convergence definition of molecular dynamics simulations solely based on the root mean square deviation possible? *J Comput Biol.* 2011; 18: 997–1005. <https://doi.org/10.1089/cmb.2010.0237> PMID: 21702691
62. Kumar CV, Swetha RG, Anbarasu A, Ramaiah S. Computational analysis reveals the association of threonine 118 methionine mutation in PMP22 resulting in CMT-1A. *Adv Bioinformatics.* 2014; 2014: 10. <https://doi.org/10.1155/2014/502618> PMID: 25400662
63. Martinez L. Automatic Identification of Mobile and Rigid Substructures in Molecular Dynamics Simulations and Fractional Structural Fluctuation Analysis. Kleinjung J, editor. *PLoS One.* 2015; 10: e0119264. <https://doi.org/10.1371/journal.pone.0119264> PMID: 25816325
64. Kuzmanic A, Zagrovic B. Determination of ensemble-average pairwise root mean-square deviation from experimental B-factors. *Biophys J.* Biophysical Society; 2010; 98: 861–871. <https://doi.org/10.1016/j.bpj.2009.11.011> PMID: 20197040
65. Craveur P, Joseph AP, Esque J, Narwani TJ, Noël F, Shinada N, et al. Protein flexibility in the light of structural alphabets. *Front Mol Biosci.* 2015; 2. <https://doi.org/10.3389/fmbo.2015.00020> PMID: 26075209

66. Yuan Z, Bailey TL, Teasdale RD. Prediction of protein B-factor profiles. *Proteins Struct Funct Genet.* 2005; 58: 905–912. <https://doi.org/10.1002/prot.20375> PMID: 15645415
67. Yang LQ, Sang P, Tao Y, Fu YX, Zhang KQ, Xie YH, et al. Protein dynamics and motions in relation to their functions: Several case studies and the underlying mechanisms. *J Biomol Struct Dyn.* 2014; 32: 372–393. <https://doi.org/10.1080/07391102.2013.770372> PMID: 23527883
68. David CC, Jacobs DJ. Principal Component Analysis: A Method for Determining the Essential Dynamics of Proteins. *Methods Mol Biol.* 2014; 1084: 193–226. https://doi.org/10.1007/978-1-62703-658-0_11 PMID: 24061923
69. Stein SAM, Loccisano AE, Firestone SM, Evanseck JD. Principal Components Analysis: A Review of its Application on Molecular Dynamics Data. *Annual Reports in Computational Chemistry.* 2006. pp. 233–248. <https://doi.org/10.1016/S1574>
70. Vinay Kumar C, Kumar KM, Swetha R, Ramaiah S, Anbarasu A. Protein aggregation due to nsSNP resulting in P56S VABP protein is associated with amyotrophic lateral sclerosis. *J Theor Biol.* Elsevier; 2014; 354: 72–80. <https://doi.org/10.1016/j.jtbi.2014.03.027> PMID: 24681403
71. Weng S-L, Huang K-Y, Kaunang FJ, Huang C-H, Kao H-J, Chang T-H, et al. Investigation and identification of protein carbonylation sites based on position-specific amino acid composition and physico-chemical features. *BMC Bioinformatics.* BMC Bioinformatics; 2017; 18: 66. <https://doi.org/10.1186/s12859-017-1472-8> PMID: 28361707
72. Kumar A, Randhawa V, Acharya V, Singh K, Kumar S. Amino acids flanking the central core of Cu,Zn superoxide dismutase are important in retaining enzyme activity after autoclaving. *J Biomol Struct Dyn.* 2015; 1–31. <https://doi.org/10.1080/07391102.2015.1049551> PMID: 25990646
73. Hubbard RE, Kamran Haider M. Hydrogen Bonds in Proteins: Role and Strength. *Encycl Life Sci.* 2010; <https://doi.org/10.1002/9780470015902.a0003011.pub2>
74. Wu J, Jiang R. Prediction of Deleterious Nonsynonymous Single-Nucleotide Polymorphism for Human Diseases. *Sci World J.* 2013;2013.
75. Guharoy M, Chakrabarti P. Secondary structure based analysis and classification of biological interfaces: Identification of binding motifs in protein-protein interactions. *Bioinformatics.* 2007; 23: 1909–1918. <https://doi.org/10.1093/bioinformatics/btm274> PMID: 17510165
76. Brigadski T, Leßmann V. BDNF: a regulator of learning and memory processes with clinical potential. *e-Neuroforum.* 2017; 20: 1–11. <https://doi.org/10.1515/s13295-014-0053-9>
77. Mizui T, Kojima M. Recent Advances in the Biology of BDNF And the Newly Identified. *J Neurol Neuro-medicine.* 2018; 3: 1–4.
78. Tettamanti G, Cattaneo AG, Gornati R, de Eguileor M, Bernardini G, Binelli G. Phylogenesis of brain-derived neurotrophic factor (BDNF) in vertebrates. *Gene.* Elsevier B.V.; 2010; 450: 85–93. <https://doi.org/10.1016/j.gene.2009.07.023> PMID: 19879341
79. Uegaki K, Kumanogoh H, Mizui T, Hirokawa T, Ishikawa Y, Kojima M. BDNF binds its pro-peptide with high affinity and the common val66met polymorphism attenuates the interaction. *Int J Mol Sci.* 2017; 18. <https://doi.org/10.3390/ijms18051042> PMID: 28498321
80. Chen Z, Patel P, Sant G, Meng C, Teng K, Hempstead B, et al. Variant Brain-Derived Neurotrophic Factor (BDNF) (Met66) Alters the Intracellular Trafficking and Activity-Dependent Secretion of Wild-Type BDNF in Neurosecretory Cells and Cortical Neurons. *J Neurosci.* 2004; 24: 4401–4411. <https://doi.org/10.1523/JNEUROSCI.0348-04.2004> PMID: 15128854
81. Narayanan V, Veeramuthu V, Ahmad-annuar A, Ramli N, Waran V, Chinna K, et al. Missense Mutation of Brain Derived Neurotrophic Factor (BDNF) Alters Neurocognitive Performance in Patients with Mild Traumatic Brain Injury: A Longitudinal Study. 2016; 1–15. <https://doi.org/10.1371/journal.pone.0158838> PMID: 27438599
82. Rostami E, Krueger F, Zoubak S, Monte OD, Raymond V, Pardini M, et al. Bdnf polymorphism predicts general intelligence after penetrating traumatic brain injury. *PLoS One.* 2011; 6: 1–13. <https://doi.org/10.1371/journal.pone.0027389> PMID: 22087305
83. Hempstead BL. Brain-Derived Neurotrophic Factor: Three Ligands, Many Actions. *Trans Am Clin Climatol Assoc.* 2015; 126: 9–19. Available: <http://www.ncbi.nlm.nih.gov/pubmed/26330656%0Ahttp://www.ncbi.nlm.nih.gov/pmc/articles/PMC4530710/> PMID: 26330656
84. Karchin R. Next generation tools for the annotation of human SNPs. *Brief Bioinform.* 2009; 10: 35–52. <https://doi.org/10.1093/bib/bbn047> PMID: 19181721
85. Schymkowitz JWH, Rousseau F, Martins IC, Ferkinghoff-Borg J, Stricher F, Serrano L. Prediction of water and metal binding sites and their affinities by using the Fold-X force field. *Proc Natl Acad Sci U S A.* 2005; 102: 10147–10152. <https://doi.org/10.1073/pnas.0501980102> PMID: 16006526
86. Bonneau R, Ruczinski I, Tsai J, Baker D. Contact order and ab initio protein structure prediction. *Protein Sci.* 2002; 11: 1937–1944. <https://doi.org/10.1110/ps.3790102> PMID: 12142448

87. Mercado N, Collier T, Sortwell C, Steele-Collier K. BDNF in the Aged Brain: Translational Implications for Parkinson's Disease. *Austin Neurol Neurosci.* 2017; 2: 1–18. <https://doi.org/10.1016/j.jalz.2016.04.002>.Prevalence